OXFORD

Temporal hierarchy of cortical responses reflects core-belt-parabelt organization of auditory cortex in musicians

Jan Benner[1,*], Julia Reinhardt[2,3], Markus Christiner[4,5], Martina Wengenroth[6], Christoph Stippich[7], Peter Schneider[1,4,5,†],

Maria Blatow[8,†,*]

[1]Department of Neuroradiology and Section of Biomagnetism, University of Heidelberg Hospital, Heidelberg, Germany,
[2]Department of Cardiology and Cardiovascular Research Institute Basel (CRIB), University Hospital Basel, University of Basel, Basel, Switzerland,
[3]Department of Orthopedic Surgery and Traumatology, University Hospital Basel, University of Basel, Basel, Switzerland,
[4]Centre for Systematic Musicology, University of Graz, Graz, Austria,
[5]Department of Musicology, Vitols Jazeps Latvian Academy of Music, Riga, Latvia,
[6]Department of Neuroradiology, University Medical Center Schleswig-Holstein, Campus Lübeck, Lübeck, Germany,
[7]Department of Neuroradiology and Radiology, Kliniken Schmieder, Allensbach, Germany,
[8]Section of Neuroradiology, Department of Radiology and Nuclear Medicine, Neurocenter, Cantonal Hospital Lucerne, University of Lucerne, Lucerne, Switzerland

*Corresponding authors: Jan Benner, Department of Neuroradiology and Section of Biomagnetism, University of Heidelberg Hospital, Im Neuenheimer Feld 400, 69120 Heidelberg, Germany. Email: benner@musicandbrain.de; Maria Blatow, Section of Neuroradiology, Department of Radiology and Nuclear Medicine, Neurocenter, Cantonal Hospital Lucerne, University of Lucerne, Spitalstrasse, 6000 Luzern 16, Switzerland. Email: maria.blatow@luks.ch

†Peter Schneider and Maria Blatow have contributed equally to this work.

Human auditory cortex (AC) organization resembles the core-belt-parabelt organization in nonhuman primates. Previous studies assessed mostly spatial characteristics; however, temporal aspects were little considered so far. We employed co-registration of functional magnetic resonance imaging (fMRI) and magnetoencephalography (MEG) in musicians with and without absolute pitch (AP) to achieve spatial and temporal segregation of human auditory responses. First, individual fMRI activations induced by complex harmonic tones were consistently identified in four distinct regions-of-interest within AC, namely in medial Heschl's gyrus (HG), lateral HG, anterior superior temporal gyrus (STG), and planum temporale (PT). Second, we analyzed the temporal dynamics of individual MEG responses at the location of corresponding fMRI activations. In the AP group, the auditory evoked P2 onset occurred ∼25 ms earlier in the right as compared with the left PT and ∼15 ms earlier in the right as compared with the left anterior STG. This effect was consistent at the individual level and correlated with AP proficiency. Based on the combined application of MEG and fMRI measurements, we were able for the first time to demonstrate a characteristic temporal hierarchy ("chronotopy") of human auditory regions in relation to specific auditory abilities, reflecting the prediction for serial processing from nonhuman studies.

Key words: Heschl's gyrus; auditory processing; absolute pitch; functional magnetic resonance imaging; magnetoencephalography.

Introduction

The human auditory cortex (AC) has been extensively investigated in anatomical and functional neuroimaging studies, which confirm AC's location in the superior temporal gyrus (STG), in particular in Heschl's gyrus (HG) and adjacent areas, including the planum polare (PP) and planum temporale (PT) (Galaburda and Sanides 1980; Melcher et al. 1999; Kaas and Hackett 2000; Hackett 2008; Woods and Alain 2009; Moerel et al. 2014; Leaver and Rauschecker 2016). The literature on nonhuman primates corroborates the existence of a hierarchical structural and functional organization of at least 13 distinct subfields within AC forming a core and surrounding belt and parabelt auditory areas (Kaas et al. 1999; Kaas and Hackett 2000; Hackett et al. 2001, 2014; Sweet et al. 2005; Hackett 2011). The three subfields within the core area receive their input from the ventral division of the medial geniculate nucleus, process auditory information in parallel, and have cytoarchitectonic and electrophysiological characteristics of primary sensory cortices. Core auditory neurons respond with short latencies to simple acoustic stimuli, show narrow receptive fields, and are modulated by basic properties of sound as intensity

and location (Kaas et al. 1999). Central auditory areas exhibit tonotopic organization, i.e. frequency-specific cortical maps that show a systematic mirror-image distribution of frequency representations from "low to high to low" (Morel et al. 1993; Rauschecker 1998; Recanzone et al. 2000; Herdener et al. 2013; Joly et al. 2014); for review, see: Schreiner and Winer (2007). Core areas of the two hemispheres are directly and strongly interconnected via transcallosal projections. The eight subfields within the belt area receive their inputs mainly from the core area and the dorsal and medial divisions of the medial geniculate nucleus and are strongly interconnected (Kaas et al. 1999; Kaas and Hackett 2000). They have cytoarchitectonic and electrophysiological characteristics of secondary cortices, are formed by neurons with higher responsiveness to complex acoustic features and broader receptive fields, and display only partial or less refined tonotopic organization (Rauschecker et al. 1995; Kaas and Hackett 2000; Hackett et al. 2001). However, there are also exceptions to these rules, as for example macaque belt area CM displays core-like physiological properties (Camalier et al. 2012). Finally, sub-fields within the parabelt area (at least two), adjacent to the belt

area along the lateral aspect of STG, receive their inputs not only from the belt areas but also from the dorsal and medial divisions of the medial geniculate nucleus and have cytoarchitectonic and electrophysiological characteristics of association cortices. Their neurons are tuned to more complex properties of sound (e.g. pitch), are strongly modulated by attention, and show no tonotopic organization (Kaas et al. 1999). Parabelt and, to a lesser degree, belt areas project to neighboring polysensory temporal, and more distant parietal and prefrontal cortices for higher levels of processing (Kaas and Hackett 2000; Hackett 2011). In general, a serial processing of auditory information from core to belt to parabelt areas is assumed (Hackett 2011) and several studies have confirmed that core areas exhibit the shortest onset latencies, while noncore areas are characterized by progressively longer latencies (Recanzone et al. 2000; Lakatos et al. 2005; Camalier et al. 2012; Nourski et al. 2014; Nourski 2017). Connectivity studies have demonstrated at least two distinct pathways originating from rostral and caudal lateral belt areas that target distinct domains of the frontal lobes. This suggests separate streams of spatial and nonspatial auditory information (Romanski et al. 1999; Kaas and Hackett 2000). However, converging evidence points to a far more complex view of the hierarchical organization of auditory information processing, which involves a dynamic whole brain network of highly interconnected auditory and auditory-related areas (Hackett 2011; Hackett et al. 2014).

Most studies in humans suggest that the basic principles of core-belt-parabelt organization of human AC are similar to those in nonhuman primates (Scheich et al. 1998; Hackett et al. 2001; Sweet et al. 2005; Woods and Alain 2009; Chevillet et al. 2011; Barton et al. 2012; Moerel et al. 2014). A number of studies have addressed the tonotopic organization of human primary AC (PAC) revealing a frequency-dependent segregation of auditory regions (Bilecen et al. 1998; Formisano et al. 2003; Talavage et al. 2004; Woods et al. 2009; Da Costa et al. 2011; Herdener et al. 2013; Leaver and Rauschecker 2016; Besle et al. 2019); for review, see: Saenz and Langers (2014). Even though anatomical landmarks are missing, there is converging evidence that PAC is mainly located in the medial 2/3 of HG and adjacent posterior duplications (Woods and Alain 2009; Da Costa et al. 2011; Moerel et al. 2012, 2014; De Martino et al. 2015; Zoellner et al. 2019), as predicted by cytoarchitectonic data (Galaburda and Sanides 1980; Morosan et al. 2001; Rademacher et al. 2001; Sweet et al. 2005; Fullerton and Pandya 2007). Functional imaging studies have shown that presumed human core auditory areas in medial HG are involved in more basic auditory analyses (Pantev et al. 1989; Seifritz et al. 2002; Formisano et al. 2003; Okada et al. 2010; Leaver and Rauschecker 2016) and sensitive to changes in basic properties of sound such as intensity (Bilecen et al. 2002; Woods et al. 2009) and location (Jäncke et al. 2002; Petkov et al. 2004; Behne et al. 2005; Woods et al. 2009). In marked contrast, presumed human belt and parabelt auditory areas in lateral HG and lateral anterior and posterior STG seem to process more complex features of sound such as pitch, melody, rhythm, and timbre as well as specific auditory, musical, and language-related components (Binder et al. 2000; Wessinger et al. 2001; Hall et al. 2002; Patterson et al. 2002; Zatorre et al. 2002; Griffiths 2003; Schneider et al. 2005; Hickok and Poeppel 2007; Okada et al. 2010; Chevillet et al. 2011; Golestani et al. 2011; Farbood et al. 2015; Allen et al. 2022); for review, see: Moerel et al. (2021).

In addition to the large number of reports investigating anatomical features and/or stimulus-dependent cortical mapping of human AC, relatively few studies have explored the temporal aspects of human auditory processing. Several

magnetoencephalography (MEG) studies have provided evidence for tonotopic organization of presumed PAC as reflected by frequency-dependent postero-medial shift of auditory-evoked fields (AEF) (Romani et al. 1982; Pantev et al. 1988; Scherg et al. 1989; Lütkenhöner et al. 2003; Wienbruch et al. 2006). Further studies have shown that the distribution of AEF latencies is generally consistent with serial processing, extending from the presumed core area into neighboring areas in STG (Liegeois-Chauvel et al. 1994; Pantev et al. 1995; Yoshiura et al. 1996). Few investigations have used intracranial electrophysiological recordings in neurosurgical patients and provided evidence for the core-belt-parabelt organization of human AC, e.g. measuring an increase of neuronal frequency preference toward postero-medial locations (Howard et al. 1996). Further results revealed the spatiotemporal pattern of activity, propagating first along the medio-lateral and then along the postero–anterior axis of the supratemporal plane (Yvert et al. 2005), or delineating three auditory subfields based on distinct shapes of auditory-evoked potentials (Brugge et al. 2008) (for review, see: Nourski 2017). Recently, Nourski et al. (2014) employed intracranial recordings to directly measure onset latencies in different regions of AC. In accordance with the predictions of results in nonhuman primates, the authors found the shortest response latencies within posteromedial HG, corroborating the assumption that it contained core auditory areas. Response latencies were found to progressively increase along the medio-lateral axis, with longer latencies in a middle portion of posterolateral STG (presumed belt), followed by surrounding areas of posterolateral STG and anterolateral HG (presumed parabelt). Moreover, a recent study using direct electrophysiological recordings investigated auditory decoding of speech and reported parallel and distributed processing within AC (Hamilton et al. 2021).

Absolute pitch (AP) is the rare ability to immediately and effortlessly identify the pitch of any given tone without relying on external reference (Zatorre 2003). The prevalence of AP is estimated to be ~0.01% in the general population, but ~7–32% in professional musicians (Baharloo et al. 1998; Gregersen et al. 1999). The quality of AP perception may depend on the stimulus material and particularly was found to be more accurate for natural complex tones as compared with sine tones (Gruhn 2018). In some individuals, partial AP qualities or instrument-specific AP is observed where AP is restricted to limited frequency ranges or facilitated by sounds produced by their own instrument (Reymore and Hansen 2020). AP possessors recognize pitch instantaneously and can label it according to musical scale with no delay. This has led to the notion that AP is based on an early step of pitch recognition, followed by a subsequent step of pitch labeling (Levitin and Rogers 2005; Elmer et al. 2015). It is assumed that the neuronal processes of pitch recognition, pitch labeling, and pitch memory involve distinct or incompletely overlapping neuronal networks (Levitin and Rogers 2005; Wilson et al. 2009; Wengenroth et al. 2014). Recent 2-component models suggest that the pitch perception in AC and the mnemonic association component of pitch labeling in the prefrontal cortex are characterized by enhanced perisylvian connectivity in AP (Jäncke et al. 2012; Elmer et al. 2015).

At the structural level, several neuroimaging studies have assessed hemispheric asymmetry of STG in musicians with AP and found significant grey matter volume differences in HG and/or PT in the right versus left hemisphere (Schlaug et al. 1995; Keenan et al. 2001; Luders et al. 2004; Wilson et al. 2009; Wengenroth et al. 2014). This has initiated controversies about the contribution of left- vs. right-hemispheric structures to

AP perception with regard to anatomical (Zatorre et al. 1998; Bermudez et al. 2009; Loui et al. 2011; Wengenroth et al. 2014) and functional aspects (Zatorre et al. 1998; Ohnishi et al. 2001; Bermudez and Zatorre 2005; Schulze et al. 2009; Wilson et al. 2009; Oechslin et al. 2010; Wengenroth et al. 2014). Tract-based structural connectivity statistics showed higher fractional anisotropy within the path of the inferior fronto-occipital, longitudinal, and uncinate fasciculus of AP musicians (Dohn et al. 2015). Recently, greater resting state functional connectivity and enhanced intracortical myelination were observed in the right PP in musicians with AP (Kim and Knösche 2016, 2017) supporting a critical role of the ventral pathway in AP recognition. At the temporal level, between-group differences could be identified within the early processing time range up to about 200 ms after tone onset in right-sided perisylvian brain regions (Wengenroth et al. 2014; Burkhard et al. 2019) and independently of the level of musical transgression (Coll et al. 2019). Using an oddball paradigm, a reduction of the later auditory-evoked P3a response could be observed in AP musicians (Rogenmoser et al. 2015), which however could not be replicated by a more recent study (Greber et al. 2018).

In this study, we selected experienced musicians with and without AP as a model population due to their generally enhanced auditory responses and high attentive capacities in the experimental setup. There is evidence that the intra- und interhemispheric timing of auditory responses may influence the quality of auditory perception already at an early processing stage (Wengenroth et al. 2014). Here, we used functional magnetic imaging (fMRI) to identify individual activations in distinct subfields of AC and MEG with a combined fit-seeding model to assess variations in the temporal hierarchical order of auditory processing during the first 90 ms after stimulus onset in musicians with and without AP. This paper describes for the first time a novel method for fMRI/MEG co-registration, which makes spatial and temporal segregation of functionally distinct auditory areas on an individual basis possible. The results illustrate that the early steps of auditory information decoding may determine the quality of auditory perception and characterize specific auditory abilities such as AP.

Materials and methods
Subjects
Forty experienced musicians participated in this study with a minimum of 5 years of instrumental practice beyond the standard school education, normal hearing level (hearing loss < 20 dB within 0.1–8 kHz), and no history of neurological disorders. All participants passed a minimum of 12 years of school and at least 4 years of academic education. Subjects included 23 musicians without AP (nonAP group) and 17 musicians with AP (AP group); see Table 1 for detailed sample description and musical background information. Musicianship related auditory skills, cognitive functions, and hearing abilities were assessed using the following psychoacoustic tests: Advanced Measures of Music Audiation test (AMMA, Gordon 1998) and Pitch Perception Preference test (Schneider et al. 2005). Subjects were matched between groups for age, gender, and total duration of musical activity (years). The AP score was significantly higher in the AP group $(t(38) = 13.53, P < 0.01)$ than in the nonAP group (Table 1). The AP group also performed significantly better in the AMMA test $(t(38) = 4.41, P < 0.01)$ and demonstrated increased mean intensity of musical activity (hours/week) as compared with the nonAP group $(t(38) = 3.38, P < 0.01)$. The AP score was significantly

correlated with the AMMA score $(r = 0.65, P < 0.01)$. All subjects gave their informed consent to participate in the experiments, which were approved by the Ethics committee of Heidelberg University.

AP test
The AP test (Wengenroth et al. 2014) was specifically designed to allow for quantification of the degree of AP ability (AP score) and consisted of 28 equally tempered (relative to standard pitch [a′] = 440 Hz) sampled instrumental test tones (piano, guitar, violin, organ, woodwind, brass, and voice) and 7 sine tones that were presented for 500 ms each in low-, middle-, and high-frequency ranges (32–138, 175–625, and 1000–2000 Hz, respectively) as well as 6 active tone production tasks. Different instrumental test tones have been chosen to address the fact that AP abilities may be influenced by timbre or register. To rule out any relative pitch-associated interval recognition, the memory of the last test tone was extinguished by intermittent interference stimuli without any harmonic relation to standard pitch: first, 5 nonequally tempered sequential instrumental tones resembling and contorting the previous test tone were presented for 500 ms each followed by 18 s of glissando-like continuously distorted music pieces (see Supplementary Materials for sound example 1). Only chroma, not octave position, was tested. For correctly identified tones 1 score point was accredited, and for semitone errors, 0.5 score point was accredited, resulting in a maximal score of 41 points. The random choice score was 6.9. The inclusion criterion for the AP group was set as the saddle point of the bimodal distribution curve ($\geq$ 21 score points).

Morphological MRI
High-resolution T_1-weighted 3D MR images of the brain (magnetization-prepared rapid acquisition of gradient echo sequence: echo time 4.38 ms, repetition time 1930 ms, 1 mm³ isotropic resolution, flip angle 15°, 176 contiguous sagittal slices, matrix size 256 mm) were acquired at 3 Tesla (Magnetom Trio, Siemens, Erlangen, Germany) with an 8-channel head coil. Additional T_2-weighted sequences were obtained and assessed by a neuroradiologist for potential pathologies. MR morphometry was computed and visualized using BrainVoyager QX 2.8 software (Brain Innovation, Maastricht, The Netherlands). T_1-weighted images were corrected for inhomogeneity, transformed into anterior commissure-posterior commissure plane, and subsequently normalized in Talairach (TAL) space (Talairach and Tournoux 1988). Subsequently, individual segmentation and 3D surface reconstruction of AC were performed based on an established procedure (Schneider et al. 2005; Benner et al. 2017). Several AC reconstructions were part of a data pool we already analyzed in previous publications (Wengenroth et al. 2014; Benner et al. 2017). In particular, the STG including HG and PT was segmented on sagittal images in a standardized semi-automatic slice-by-slice approach (Schneider et al. 2005, 2009; Wengenroth et al. 2010, 2014; Seither-Preisler et al. 2014). We employed the following criteria for anatomical AC landmarks in accordance with established criteria (Schneider et al. 2005; Abdul-Kareem and Sluming 2008; Marie et al. 2015) and by extending earlier standard definitions (Steinmetz et al. 1989; Rademacher et al. 1993, 2001; Penhune et al. 1996, 2003; Leonard et al. 1998; Kim et al. 2000; Yoshiura et al. 2000; Wong et al. 2008): the first anterior HG was defined as the most anterior transverse gyrus of STG located between the first transverse sulcus and the first transverse Heschl's sulcus (HS). For all HG morphotypes including duplications (common stem duplication, complete posterior

Table 1. Sample description and musical background.

	AP (N = 17)	nonAP (N = 23)
Age	36.5 ± 3.7	31.3 ± 2.2
Gender (f/m)	8/9	11/12
Musical status (pro/ama)	13/4	6/17
AP score	32.0 ± 1.5*	9.1 ± 0.9
AMMA score	35.1 ± 0.8*	29.3 ± 1.0
Total duration of musical activity (years)	17.6 ± 3.1	17.4 ± 3.3
Mean intensity of musical activity (hours/week)	18.4 ± 2.6*	8.7 ± 1.5
Main musical instrument (played by N subjects)	piano (13)	piano (2)
	organ (1)	organ (1)
	violin (0)	violin (5)
	cello (2)	cello (1)
	guitar (0)	guitar (4)
	woodwind (1)	woodwind (4)
	brass (0)	brass (2)
	drums (0)	drums (1)
	singing (0)	singing (3)

Subject and musicianship related data (M ± SE) are presented for each group. AP, absolute pitch; nonAP, nonabsolute pitch; f, female; m, male; pro, professional musicians; ama, amateur musicians; *$P < 0.001$.

duplication, multiple duplication), transverse gyri posterior to aHG and anterior to the first complete HS (cHS) were considered part of HG. Adjacent convolutions separated from HG by cHS were considered part of PT. The PT was defined as the cortical structure posterior to the cHS. The posterior border of PT was defined as the origin of the ascending ramus (if present), the medial border was the insular cortex, and the inferior border was the supratemporal sulcus.

Functional MRI

Block designed blood-oxygen-level-dependent (BOLD) fMRI (echo planar imaging EPI sequences, 36 oblique slices parallel to the Sylvian fissure, slice thickness 3 mm, gap 1 mm, echo time 30 ms, repetition time 2500 ms) was performed during auditory stimulation with different sampled instrumental and synthetically generated complex harmonic tones (Wengenroth et al. 2014) presented for 12:25 min in total (stimulus length 500 ms, 20 items per block, block duration 20 s, baseline: rest). Subjects were instructed to attentively listen to the presented sounds (see Supplementary Materials for sound example 2). The experimental setup was optimized for reducing the scanner noise level using acoustically optimized MRI-headphones (MR Confon OPTIME1, ~25 dB passive attenuation), standard earplugs (~20 dB attenuation), as well as foam cushions additionally installed around the headphones (~15 dB attenuation). Auditory stimuli were also level adjusted for an optimal signal to noise ratio during the MRI scan. Subsequently to motion correction, slice timing correction, alignment, and TAL transformation, all functional maps were superimposed on both the structural 3D datasets and the 3D surface reconstructions of individual AC using BrainVoyager QX 2.8 software. Auditory stimulation was contrasted with the baseline condition (no tone, rest). BOLD activations were analyzed individually and related to each subject's individual HG morphotype including HG duplications. Four distinct regions of interest (ROIs) within AC were defined, namely medial HG/medial HG duplication (ROI 1), lateral HG/lateral HG duplication (ROI 2), anterior STG (ROI 3), and PT (ROI 4). For standardized individual analysis of functional data, a dynamic thresholding evaluation routine was used (Blatow et al. 2007, 2009, 2011; Stippich et al. 2007). A minimal cluster size of 4 (BrainVoyager QX standard preset) was used as a spatial filter, e.g. clusters below this size were not displayed in the

activation map. This standard cluster size for data evaluation was previously empirically established: it proved to be large enough to eliminate very small clusters resulting from artificial noise (false positives) and small enough to enable precise functional–anatomical correlation. At first, a very high statistical threshold value for the correlation between the measured BOLD signals and the hemodynamic reference function (hrf) was selected so that no functional activation was displayed (empty map). This threshold was then continually reduced. As a result, the activation with the highest correlation to the hrf that exceeded the cluster size of 4 was displayed first. By further reduction of the threshold, activations with lower correlations between the measured BOLD signals and the hrf appeared progressively. This procedure was continued until activations were identified in all ROIs. A statistical threshold of $P < 0.05$ (FDR corrected) was established as a lower limit to ensure that BOLD signals were clearly distinguishable from background noise. If no BOLD signal was displayed in a ROI within the lower limit, this was evaluated as "no activation". Likewise, BOLD signals with a relative signal change of > 4% were not included in the evaluation because such high-level activation is likely to originate from draining veins rather than from capillaries (Peeters and Sunaert 2007). In each ROI, the center of gravity of the BOLD signal was evaluated at the highest possible threshold assessing spatial coordinates and t-value.

Magnetoencephalography

AEF were recorded using a Neuromag-122 whole-head MEG system in response to different sampled instrumental and synthetically generated complex harmonic tones in analogy to the fMRI experiment. Subjects were instructed to attentively listen to the sounds, each of which was presented 200 times in pseudo-randomized order (tone length 500 ms, interstimulus interval range 400–600 ms). AEF were recorded with a sampling rate of 1000 Hz and were limited by an adequate 330 Hz lowpass filter (DC). Data analysis was conducted with the BESA Research 6.0 software (MEGIS Software GmbH, Graefelfing, Germany). Prior to averaging, data were automatically checked to exclude external artifacts by event-related fields ERF module. By applying the automatic Artifact Scan tool, on average, about 3–7 noisy (bad) channels were excluded and about 10% of all epochs exceeding

a gradient of 600 fT/cm*s and amplitudes either exceeding 3000 fT/cm or falling below 100 fT/cm were rejected from further analysis. Thereby, a major part of endogenous artifacts, such as eye blinks, eye movements, cardiac activity, face movements, and muscle tensions, could be accounted for. A baseline-amplitude calculated over the 100ms interval before the onset of the tones was subtracted from the data. The responses of each subject were first collapsed into a grand average (2600 artifact-free epochs) in a 100ms prestimulus to 400ms poststimulus time window. To analyze onset and peak latencies of MEG responses at the location of the fMRI activations, a novel fMRI-based combined fit-seeding model was established. Individual spatial coordinates of BOLD activations in the four ROIs in AC were used as seeding points for source modeling. In cases where BOLD activations were missing within the ROI, mean spatial coordinates were employed. Dipole orientation was fitted according to the subject's individual anatomy to obtain maximal positivity of the first response. In each hemisphere, four equivalent dipoles were employed (one for each ROI). To separate the early, middle, and late components of the MEG response, e.g. (i) the P30 peaking around 20–50 ms after tone onset, (ii) the P1/N1 complex around 50–120 ms, and (iii) the P2 and P2a around 120–250 ms, time windows for source modeling were adjusted accordingly to 20–50, 50–120, and 120–250 ms, respectively. AEF could not be analyzed in 4 subjects (out of 23) of the nonAP and 1 subject (out of 17) of the AP group, due to low MEG signal power.

Statistics

Statistical analyses were performed using SPSS 24 software (IBM Corp., Armonk, NY, USA); data are presented as mean with standard error (M ± SE), unless otherwise noted. Statistical significance of differences between groups was assessed using t-tests. Paired t-tests were computed to isolate innergroup differences in fMRI and MEG parameters between hemispheres for each fMRI ROI and corresponding MEG response separately. Pearson's coefficients were used for correlational analyses and, such as the t-tests, corrected for their overall false discovery rate by applying a Benjamini–Hochberg correction $P \leq 0.05$. Cross-correlations of P1 versus P2(a) source-waveforms were calculated using MATLAB software (R2020b, The MathWorks Inc.).

Results
BOLD activations in anatomically distinct cortical areas of AC

Block-designed fMRI using auditory stimulation with instrumental and synthetic tones of a wide frequency range in an attentive listening paradigm, optimized for robust individual BOLD signals, was performed in 23 musicians. Statistical parametric maps were analyzed individually using a standardized dynamic thresholding routine (Blatow et al. 2007, 2009, 2011; Stippich et al. 2007). Starting from an empty map (highest threshold), statistical thresholds were dynamically adjusted according to each subject's activation level, until distinct clusters of activation appeared in STG (Fig. 1a and b). Individual clusters were analyzed at a statistical threshold of at least $P < 0.05$ (FDR corrected). FMRI activation maps were first projected onto 3D anatomical planes for inspection and then rendered onto individually segmented 3D surface reconstructions of each subject's STG to better visualize activations on the cortical surface and relate them to individual anatomy, in particular to sulcal boundaries (Fig. 1c and d). Using anatomical criteria established in our previous studies (Schneider et al. 2005; Benner et al. 2017), four ROIs were defined: medial HG /

medial HG duplication (ROI 1), lateral HG / lateral HG duplication (ROI 2), anterior STG (ROI 3), and PT (ROI 4). BOLD activations were consistently found in all four ROIs in all subjects, albeit with different occurrence probabilities. The highest probability of activation was found in ROI 2 with 98%, lower probabilities were found in ROIs 1, 3, and 4 (with 59%, 57%, and 52%, respectively). When more than one activation cluster was found in an ROI, the strongest cluster was evaluated. The spatial distribution of BOLD activations was similar in both hemispheres. Small asymmetries were observed in the y-axis, reflecting the known anatomical asymmetry of left/right STG (Fig. 1e). In the nonAP group, signal strength (measured as t-value) was on average comparable across all ROIs showing slightly lower values in ROI 3 and 4 (n.s.) as compared with ROI 1 and 2 (Fig. 1f). Spatial coordinates and t-values of BOLD activations are summarized in Table 2.

MEG responses in four distinct ROIs in AC display chronotopic organization

MEG with acoustic stimuli analogous to the fMRI experiment was performed in the same 23 musicians. Individual data analysis was conducted in a subgroup of 19 subjects (see Methods) applying a novel fMRI-based combined fit-seeding model to analyze onset and peak latencies of MEG responses at the location of the fMRI activations. Individual spatial coordinates of BOLD activations in the four ROIs in AC were used as seeding points for source modeling. In cases where BOLD activations were missing within the ROI, mean spatial coordinates were employed (Fig. 2a). Dipole orientation was fitted according to the subject's individual anatomy to obtain maximal positivity of the first response (Fig. 2b). In each hemisphere, four dipoles were employed (one for each ROI). To separate the early, middle, and late MEG components (P30 / P1–N1 / P2 & P2a), time windows for source modeling were adjusted accordingly to 20–50, 50–120, and 120–250 ms, respectively. In each ROI, a distinct average source waveform was obtained (Fig. 2c). By measuring onset and peak latencies of the evoked responses (ms after stimulus onset), a chronotopic order of responses could be detected in the four ROIs. The earliest primary response (P30) localized to medial HG (ROI 1) with an average onset latency of ~20 ms, the secondary response (P1-N1 complex) to the lateral HG (ROI 2) with an onset latency of ~28 ms and the later P2 and P2a responses to the anterior STG and PT, respectively, with onset latencies of ~51 and ~57 ms (ROIs 3 and 4, Fig. 2d). Average latencies of the first peak were ~34, ~63, ~87, and ~90 ms for ROI 1–4, respectively. Source waveform parameters are summarized in Table 3.

Preceding P2 and P2a responses in right versus left AC in musicians with AP

Analogous fMRI and MEG experiments were performed in 17 musicians with AP (1 subject was excluded from MEG analysis, see Methods). BOLD activations were consistently found in the four ROIs in all subjects, with similar occurrence probabilities as in the nonAP group. The highest probability of activation was found in ROI 2 with 94%, lower probabilities were found in ROIs 1, 3, and 4 (with 74%, 62%, and 59%, respectively). The spatial distribution of BOLD activations was similar in both hemispheres and comparable to the nonAP group. The small asymmetries in the y-axis observed in the nonAP group were less pronounced in the AP group, presumably reflecting the known right hemispheric dominance of AC in this population (e.g. less left/right asymmetry; Fig. 3a). Signal strength (measured as t-value) in each ROI did not differ on average significantly between groups (AP vs. nonAP) or hemispheres within the groups (left vs. right). In
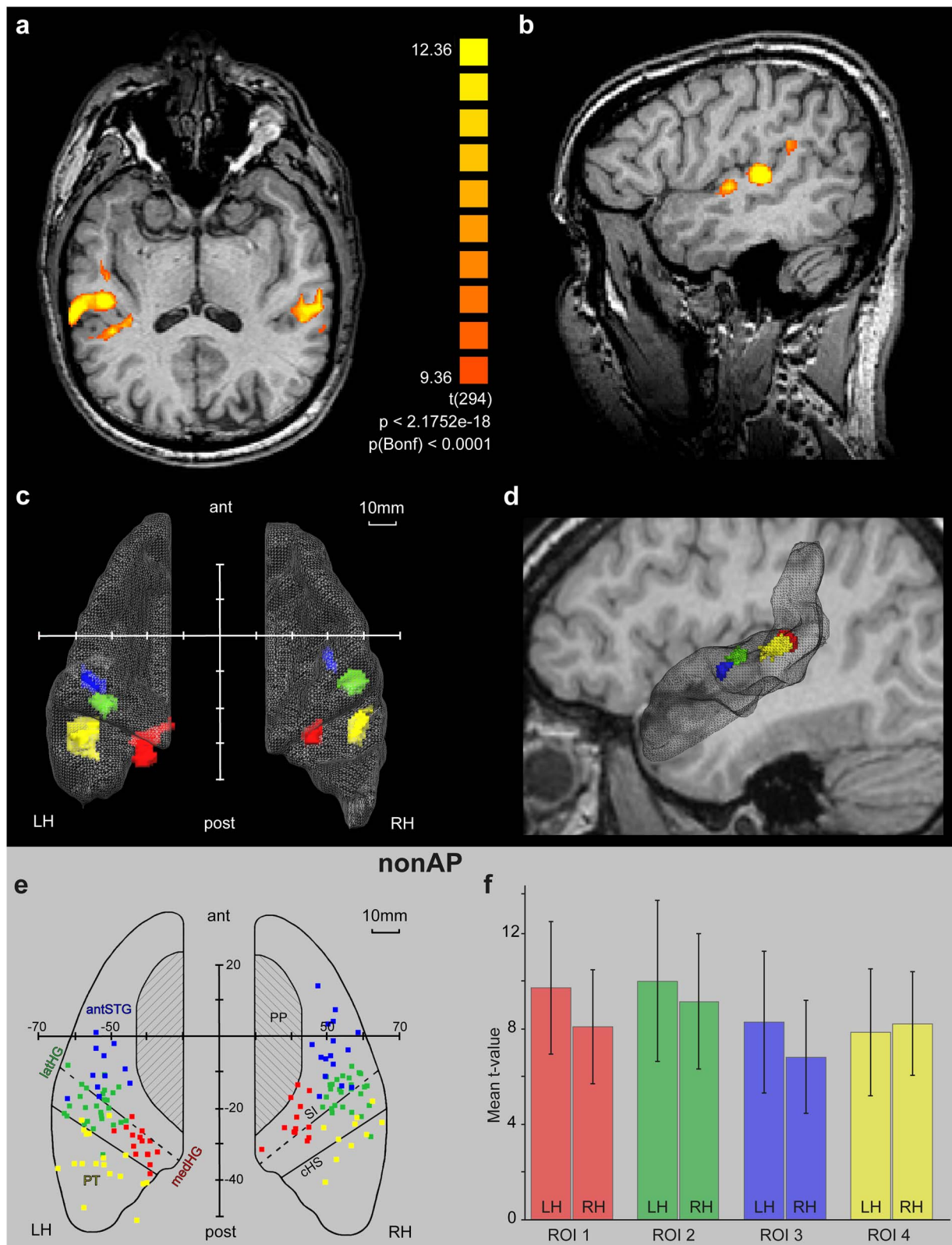
Fig. 1. BOLD activations occur in four distinct ROIs in AC of musicians. Exemplary individual BOLD activation clusters in the AC during auditory fMRI task (individual threshold) superimposed on a) axial and b) sagittal MRI planes. 3D reconstruction of exemplary STG (mesh) shown in c) axial and d) sagittal views, containing individual color-coded auditory BOLD activation clusters. Four distinct ROIs were defined and color-coded based on the corresponding anatomical area of each cluster: ROI 1: Medial HG (red), ROI 2: Lateral HG (green), ROI 3: Anterior STG (blue), ROI 4: PT (yellow). e) Individual positions of BOLD activations within the ROIs in nonAP musicians were marked onto the axial plane of a schematic AC using TAL coordinates of the center of gravity (not representing the actual cluster size). f) Histograms depict mean (± SD) BOLD *t*-values for each ROI and hemisphere in the nonAP group. nonAP, nonabsolute pitch; medHG, medial Heschl's gyrus; latHG, lateral Heschl's gyrus; antSTG, anterior superior temporal gyrus; PT, planum temporale; SI, sulcus intermedius; cHS, complete Heschl's sulcus; TAL, Talairach; ant, anterior; post, posterior; LH / RH, left/right hemisphere.

Table 2. FMRI parameters.

AP

ROI	LH				RH			
	t-value	x	y	z	t-value	x	y	z
1	8.2 ± 0.7	−40.6 ± 1.3	−33.4 ± 1.5	11.8 ± 1.3	8.0 ± 0.7	43.2 ± 1.6	−28.7 ± 1.8	13.1 ± 0.9
2	10.0 ± 0.8	−54.4 ± 1.3	−23.8 ± 1.6	7.8 ± 1.0	9.8 ± 0.7	57.0 ± 1.1	−19.8 ± 1.5	10.9 ± 0.9
3	7.2 ± 0.8	−53.0 ± 0.9	−9.2 ± 2.3	1.7 ± 0.9	5.9 ± 0.3	51.9 ± 1.4	−5.7 ± 2.1	2.7 ± 1.1
4	9.6 ± 1.1	−54.6 ± 2.2	−34.3 ± 2.5	13.5 ± 1.6	8.9 ± 0.8	59.0 ± 1.8	−31.9 ± 1.2	15.9 ± 1.6

nonAP

ROI	LH				RH			
	t-value	x	y	z	t-value	x	y	z
1	9.7 ± 0.7	−42.7 ± 0.8	−29.4 ± 1.0	8.8 ± 1.0	8.1 ± 0.7	42.2 ± 1.0	−23.5 ± 1.6	10.8 ± 1.3
2	10.0 ± 0.7	−54.0 ± 1.0	−19.0 ± 0.9	5.3 ± 0.6	9.2 ± 0.6	56.0 ± 0.8	−15.3 ± 1.0	6.7 ± 0.7
3	8.3 ± 0.9	−53.0 ± 1.4	−9.0 ± 1.9	1.2 ± 1.0	6.8 ± 0.6	52.2 ± 0.9	−3.8 ± 2.2	1.8 ± 1.0
4	7.8 ± 0.7	−53.7 ± 2.0	−32.8 ± 1.7	10.5 ± 1.0	8.2 ± 0.7	56.6 ± 1.8	−28.6 ± 2.1	12.2 ± 1.8

Mean fMRI *t*-values and TAL coordinates in mm (M ± SE) are presented per group for each ROI and hemisphere. AP, absolute pitch; nonAP, nonabsolute pitch; LH/RH, left/right hemisphere.

Table 3. MEG parameters.

AP

ROI	LH			RH		
	onset (ms)	peak (ms)	amplitude (nAm)	onset (ms)	peak (ms)	amplitude (nAm)
1	18.0 ± 0.9	32.8 ± 1.0	11.0 ± 1.5	17.2 ± 0.9	32.9 ± 0.9	12.7 ± 1.5
2	23.6 ± 0.7	61.6 ± 1.0	17.9 ± 2.1	24.9 ± 0.6	61.3 ± 1.6	17.8 ± 2.0
3	46.0 ± 3.4	79.8 ± 3.7	10.2 ± 1.0	30.4 ± 3.0	57.9 ± 3.6	10.7 ± 1.2
4	55.8 ± 2.7	90.5 ± 2.7	8.2 ± 1.1	29.1 ± 1.4	46.9 ± 2.6	8.1 ± 0.7

nonAP

ROI	LH			RH		
	onset (ms)	peak (ms)	amplitude (nAm)	onset (ms)	peak (ms)	amplitude (nAm)
1	19.6 ± 0.8	33.7 ± 1.3	11.2 ± 1.7	20.0 ± 1.1	34.4 ± 1.5	11.6 ± 1.4
2	27.4 ± 1.0	62.8 ± 2.3	14.8 ± 2.0	29.3 ± 1.2	63.7 ± 2.7	10.6 ± 1.4
3	50.9 ± 3.3	85.0 ± 4.9	10.1 ± 1.2	50.6 ± 3.0	89.1 ± 4.3	10.3 ± 1.0
4	58.1 ± 2.2	90.0 ± 3.8	8.0 ± 1.0	56.2 ± 2.0	90.8 ± 3.1	10.7 ± 1.2

Mean MEG response parameters (M ± SE) are presented per group for each ROI and hemisphere. AP, absolute pitch; nonAP, nonabsolute pitch; LH/RH, left/right hemisphere.

the AP group, *t*-values were on average higher in ROI 2 and 4 as compared with ROI 1 and 3. Within the left hemispheres, *t*-values in ROI 2 (M = 10.15, SE = 0.98) were significantly higher than in ROI 1 (M = 7.99, SE = 0.76, *t*(11) = -4.66, *P* < 0.001); as well as *t*-values in ROI 2 (M = 10.34, SE = 1.05) were significantly higher than in ROI 3 (M = 6.66, SE = 1.91, *t*(8) = 5.25, *P* < 0.001). Within the right hemispheres, no significant signal strength differences were found between the ROIs (Fig. 3b). Spatial coordinates and *t*-values of BOLD activations for the AP group are summarized in Table 2.

MEG source modeling applying the same fMRI-MEG co-registration method as in the nonAP group yielded similarly distinct average source waveforms for each ROI. As previously described (Wengenroth et al. 2014), the second peak amplitude of the late P2a component was increased in the right as compared with the left PT in musicians with AP, demonstrating reproducibility of the result with this model (Fig. 3c). Onset latencies of the evoked responses in the four ROIs were comparable to those of

nonAP musicians in the left hemisphere: the earliest primary response (P30) localized to left medial HG (ROI 1) with an average onset latency of ∼18 ms, the secondary response (P1-N1 complex) to the left lateral HG (ROI 2) with an onset latency of ∼24 ms, and the later P2 and P2a responses to the left anterior STG and PT, respectively, with onset latencies of ∼46 and ∼56 ms (ROIs 3 and 4). Latencies of the first peak in the left hemisphere of AP musicians were comparable to those of nonAP musicians in ROIs 1 and 2 with ∼33 and ∼61 ms, respectively, but were on average 20 ms shorter in ROIs 3 and 4 with ∼69 and ∼69 ms, respectively. In the right hemisphere, however, onset latencies were ∼17 ms for the primary response (ROI 1), ∼25 ms for the secondary response (ROI 2), and ∼30 and ∼29 ms for the later P2 and P2a responses (ROIs 3 and 4) in AP musicians (Fig. 3d). Thus, the onsets of late P2 and P2a responses in anterior STG and PT occurred significantly earlier in the right than in the left hemisphere of AP musicians (P2: *P* < 0.001; P2a: *P* < 0.0001). Latencies of the first peak in the right hemisphere were ∼33, ∼61,
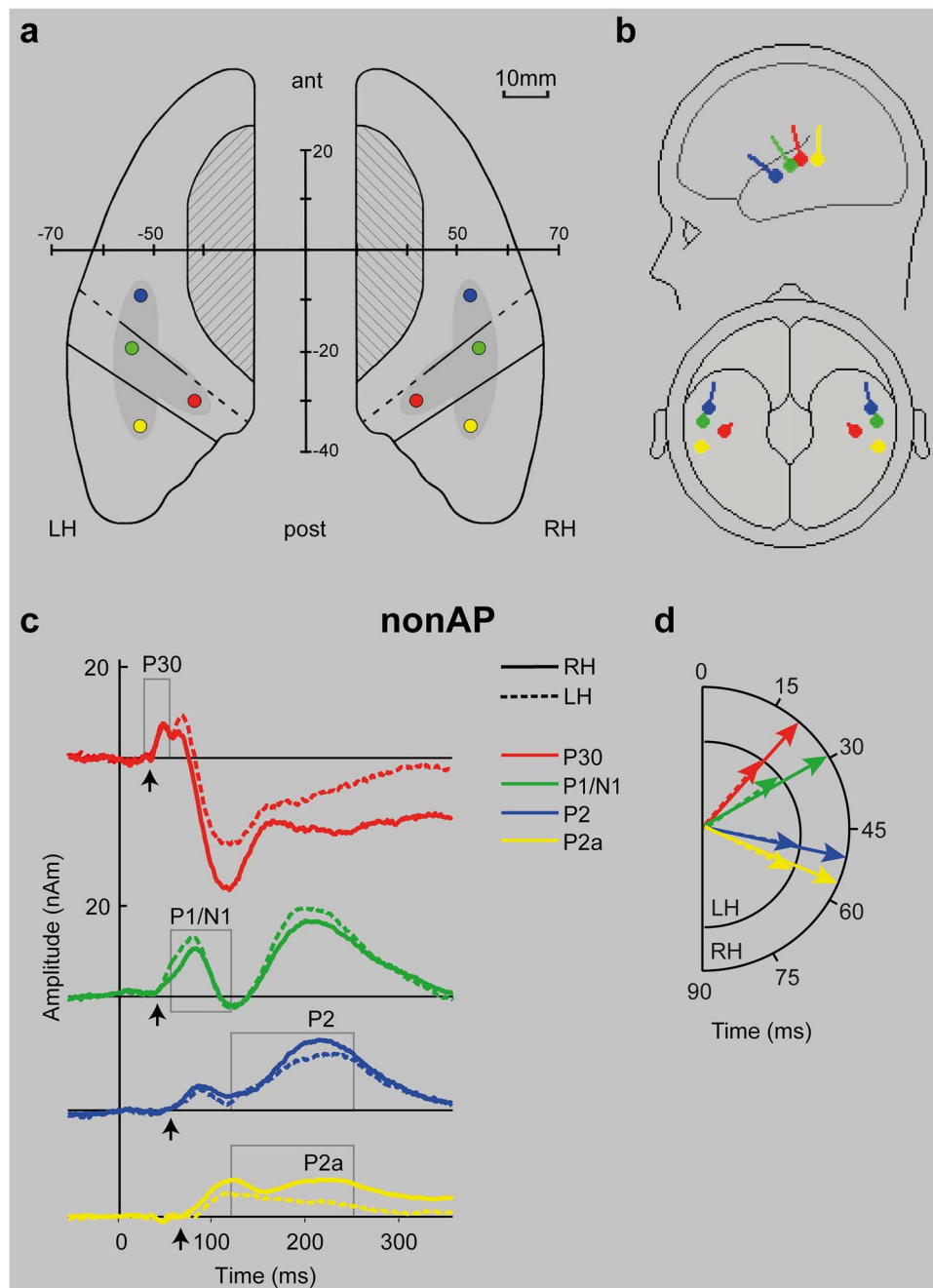
Fig. 2. Chronotopic organization of AC is reflected by distinct MEG responses in the four ROIs. a) Axial plane of schematic AC containing the exemplary positions of BOLD activations in all four ROIs as marked by colored dots (ROI 1: Red, ROI 2: Green, ROI 3: Blue, ROI 4: Yellow). b) Corresponding dipole positions in all four ROIs after co-registration on the MEG system and adaptation of dipole orientation based on individual anatomy, as marked by colored dipole-markers on a schematic head. c) Mean source waveforms of corresponding MEG responses (AEF) of the nonAP group are depicted for each ROI and hemisphere (red: P30, green: P1/N1 complex, blue: P2, yellow: P2a). Arrows mark the onsets of each response, emphasizing the left–right synchronous onset latencies between the early (P30, P1/N1) and later (P2, P2a) responses. Frames indicate the adjusted time windows for MEG source modeling (P30: 20–50 ms, P1/N1: 50–120 ms, P2(a): 120–250 ms). d) Time sequence of the mean onsets of all four MEG responses in the nonAP group, demonstrating the chronological order of auditory processing: P30 (ROI 1) – P1/N1 (ROI 2) – P2 (ROI 3) and P2a (ROI 4). nonAP, nonabsolute pitch; LH/RH, left/right hemisphere; ant, anterior; post, posterior.

~58, and ~47 ms in ROI 1–4, respectively. Hence, the peaks of the late P2 and P2a responses also occurred significantly earlier in the right than in the left hemisphere of AP musicians (P2: $P < 0.0001$; P2a: $P < 0.0001$). Furthermore, onset and peak latencies of right hemispheric P2 and P2a responses in AP musicians were significantly shorter compared with the corresponding right hemispheric responses of nonAP musicians (onset latencies P2: $P < 0.0001$; P2a: $P < 0.000001$; peak latencies P2: $P < 0.00001$; P2a: $P < 0.000001$). These effects remained significant after Bonferroni

correction for multiple testing. In marked contrast to the AP group, no significant interhemispheric differences in the nonAP group were observed. Source waveform parameters for the AP group are summarized in Table 3.

The synchronization of right auditory areas correlates with AP proficiency

At the individual level, a preceding response in the right PT (P2a, ROI 4), e.g. the response occurred earlier in the right vs. the left
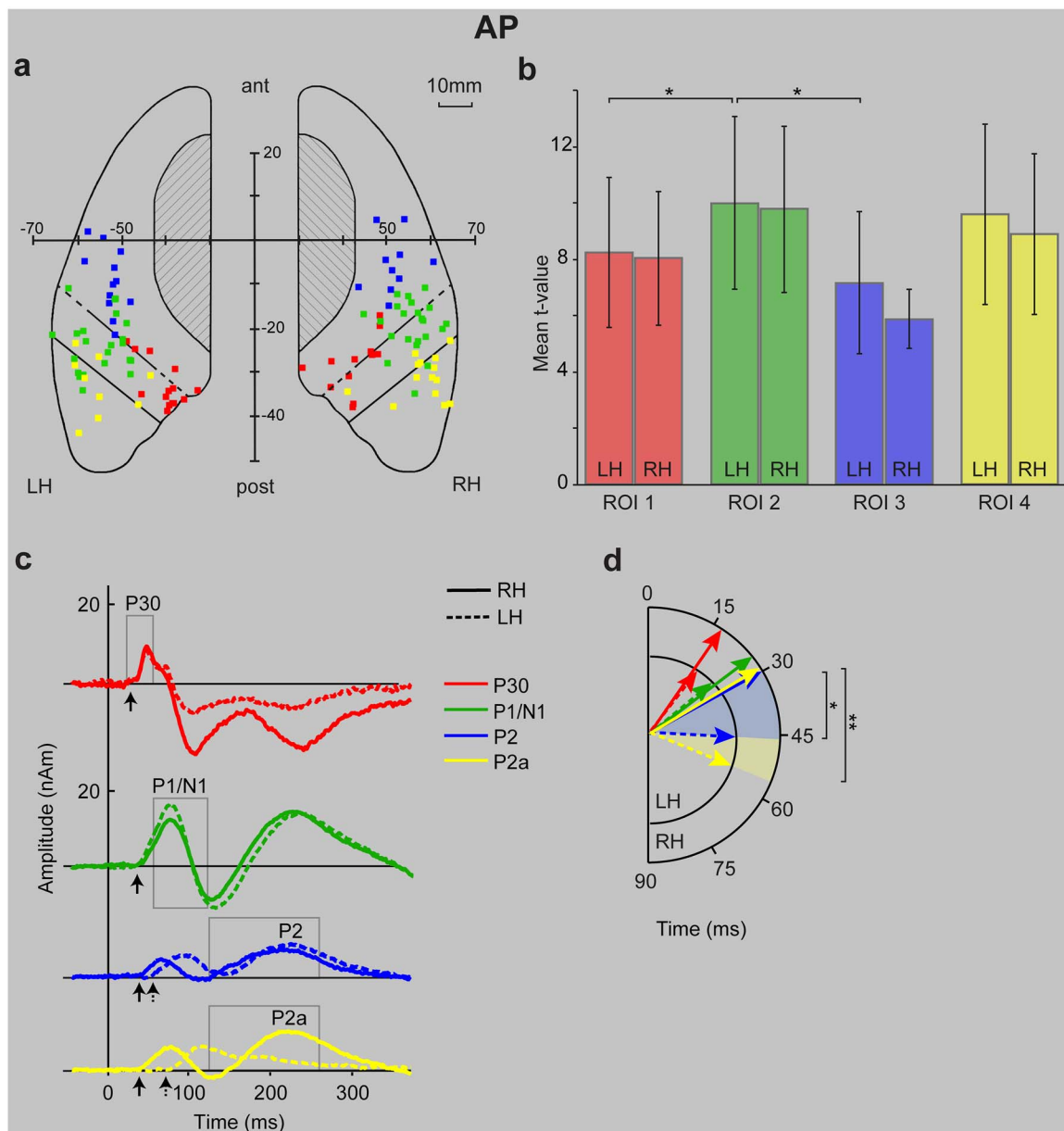
Fig. 3. Preceding P2 and P2a responses in right versus left AC in musicians with AP. a) Individual positions of BOLD activations of all AP musicians were marked onto the axial plane of a schematic AC using TAL coordinates of the center of gravity (not representing the actual cluster size). b) Histograms of the mean (± SD) BOLD *t*-values for each ROI and hemisphere of the AP group, particularly showing larger mean *t*-values of ROI 2 (lateral HG) as compared with ROI 1 (medial HG) and 3 (anterior STG). c) Mean source waveforms of corresponding MEG responses (AEF) of the AP group are depicted for each ROI and hemisphere (red: P30, green: P1/N1 complex, blue: P2, yellow: P2a). Arrows mark the onsets of each response, emphasizing the AP specific left–right onset latencies of the later P2 (anterior STG) and P2a (PT) responses. Frames indicate the adjusted time windows for MEG source modeling (P30: 20–50 ms, P1/N1: 50–120 ms, P2(a): 120–250 ms). d) Time sequence of the mean onsets of all four MEG responses in the AP group, highlighting the AP specific markedly preceding P2 and P2a responses in the right hemisphere. AP, absolute pitch; TAL, Talairach; LH/RH, left/right hemisphere; ant, anterior; post, posterior; *$P < 0.001$; **$P < 0.0001$.

hemisphere and earlier in AP vs. nonAP (Fig. 3d), was consistently found in all AP musicians (AP score $\geq$ 21) and only in one nonAP musician (AP score $\leq$ 20). For the preceding response in anterior STG (P2, ROI 3), the individual results looked more variable: in 15/17 AP musicians, the P2 response preceded either in the right vs. left hemisphere or in both hemispheres (onset latency ~30–40 ms after stimulus onset), which was also the case in 5/23 nonAP musicians (Fig. 4). Correlations of the AP score with onset latency difference (left–right) and peak latency difference (left–right) separated the two groups for P2 (onset: $r = 0.53$, $P < 0.001$, peak: $r = 0.67$, $P < 0.001$, Fig. 5a) and even more significantly for

P2a responses (onset: $r = 0.78$, $P < 0.0001$, peak: $r = 0.83$, $P < 0.0001$, Fig. 5b). The AP score was significantly correlated with the P2 onset ($r = 0.51$, $P < 0.01$), the P2 peak ($r = 0.57$, $P < 0.01$), the P2a onset ($r = 0.78$, $P < 0.01$), the P2a peak ($r = 0.80$, $P < 0.01$), and the P1/N1 amplitude ($r = 0.47$, $P < 0.01$) in the right hemisphere. In the left hemisphere, no significant correlations with AP score were found. The correlations remained significant after applying a Benjamini–Hochberg correction for overall false discovery rate $P \leq 0.05$. Cross-correlations of the source waveforms (time range 20–120 ms after stimulus onset) of the P1 response (ROI 2) with the P2 (ROI 3) or P2a response (ROI 4) showed a clear peak
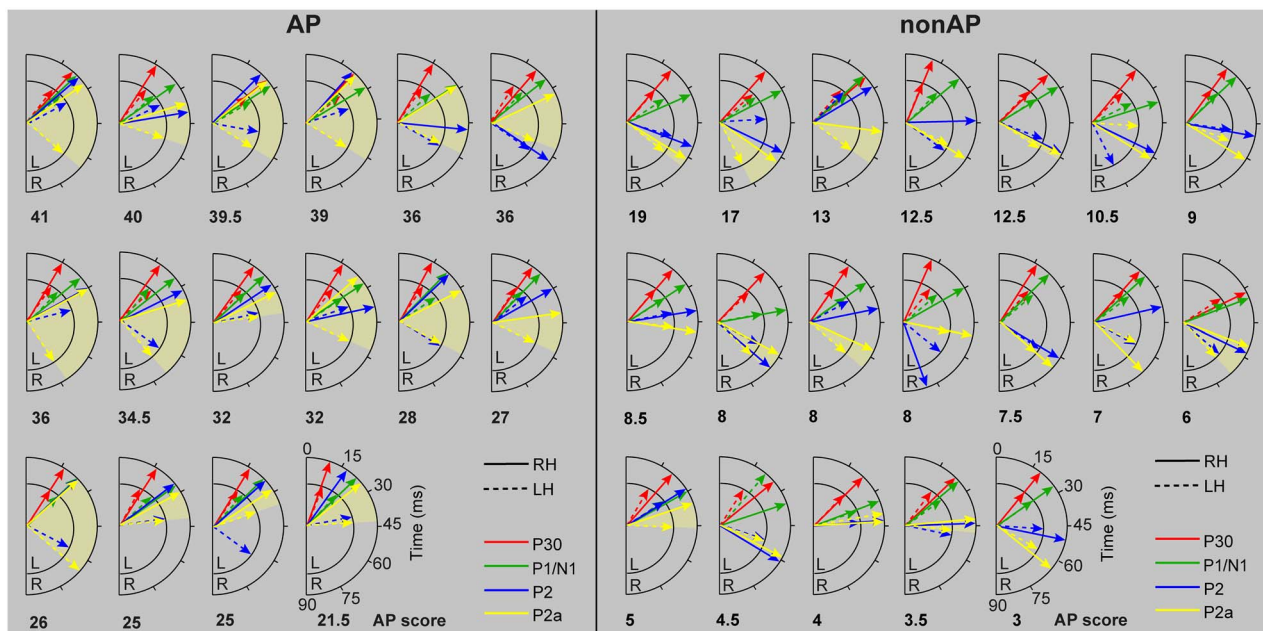
Fig. 4. Individual time sequences of MEG responses in AP and nonAP musicians. Individual time sequences of the onsets of all four MEG responses are depicted for AP (left panel) and nonAP (right panel) musicians, sorted by AP score. Left–right onset differences of the late P2a (PT) response are highlighted by the yellow area. All musicians of the AP group demonstrate a preceding right hemispheric P2a response. AP, absolute pitch; nonAP, nonabsolute pitch; LH/RH, left/right hemisphere.

synchronization in the AP-group in the right hemisphere, but not in the left hemisphere and not in the nonAP group (Fig. 5c). This was also detectable in most subjects at the individual level (Fig. 5d).

Discussion
Chronotopy

In this study, we systematically employed fMRI/MEG co-registration to characterize the spatial organization and temporal hierarchy of evoked auditory processing in human AC. Auditory information has been previously shown to proceed from medial HG over lateral HG and then to spread toward aSTG and PT, which mirrors the serial auditory processing observed in nonhuman studies (Nourski et al. 2014). The human AC exhibits important interindividual macro-anatomical variability with respect to size, shape, and gyrification (Rademacher et al. 2001; Okada et al. 2010; Chevillet et al. 2011; Barton et al. 2012; Moerel et al. 2014; Leaver and Rauschecker 2016; Benner et al. 2017; Zoellner et al. 2019). Longitudinal studies in children and young adults show remarkable stability of macro-anatomical features of AC and demonstrate clearly that this variability can only be explained by disposition (Seither-Preisler et al. 2014), Schneider P unpublished data). At the functional level, there is evidence for a hierarchical organization of subareas in primary core, secondary belt, and tertiary parabelt regions (Moerel et al. 2014; Glasser et al. 2016; Gulban et al. 2020). Recent fMRI studies have demonstrated that topographic gradients of frequency preference, e.g. tonotopy are extended along at least two orthogonal axes in human AC, oriented on the one hand in mediolateral direction along HG and, on the other hand, in anterior–posterior direction along STG (Herdener et al. 2013; Leaver and Rauschecker 2016; Moerel et al. 2021; Allen et al. 2022). Along these axes characteristic, spatial maps such as the tonotopic or periodotopic organization are found and spread the core, belt, and parabelt areas in human (Da Costa et al. 2011; Nourski et al. 2014; Besle et al. 2019) and also

nonhuman AC (Joly et al. 2014). Studies in experienced listeners such as musicians point to left–right-hemispheric asymmetries of the localization and spatial organization of primary and secondary auditory subareas (Pfeifer 1936; Zoellner et al. 2019).

However, little is known about the temporal dynamics of human auditory processing. The reasons for the lack of knowledge in this area are diverse, as for instance, invasive electrophysiological studies are challenging and rare (Nourski 2017), fMRI does not provide the necessary temporal resolution, and most MEG experiments do not discern various sources within AC (Scherg 1990; Hall et al. 2014). The temporo-spatial representation of AEF has been particularly evidenced by MEG source localization (Scherg 1984, 1990; Scherg and Berg 1991, 1996; Yoshiura et al. 1995; Godey et al. 2001; Kwon et al. 2002); however, the specific relationship between temporal and spatial aspects in the hierarchical organization of human AC remained still unclear. Neurophysiological studies based on either MEG or EEG are characterized by an excellent temporal resolution of the corresponding sources of the core or belt areas but exhibit methodological limitations due to lacking spatial information (Kanno et al. 1996; Okamoto et al. 2009; Reite et al. 2009; Okamoto et al. 2012; Shaw et al. 2013; Tang et al. 2016; Ruggles et al. 2018). Combining MEG/EEG with imaging methods such as MRI or fMRI (Lehongre et al. 2013; Hall et al. 2014; Coffey et al. 2017) facilitated to resolve AC activity with increased accuracy. However, to our knowledge, no studies exist using specific anatomically or functionally defined coordinates in the brain prior to the MEG/EEG source analysis algorithms.

Combining the high temporal resolution of MEG and the high spatial resolution of fMRI with individual data analysis, we defined individual "seeds" for the core, belt, and parabelt sources in AC. Thereby, we were able to measure with high precision and noninvasively the temporal hierarchy ("chronotopy") of primary and secondary auditory responses. Our findings corroborate the division into 2 spatio–temporal axes within AC. Based on the fMRI data, we identified four spatially separable processing loci
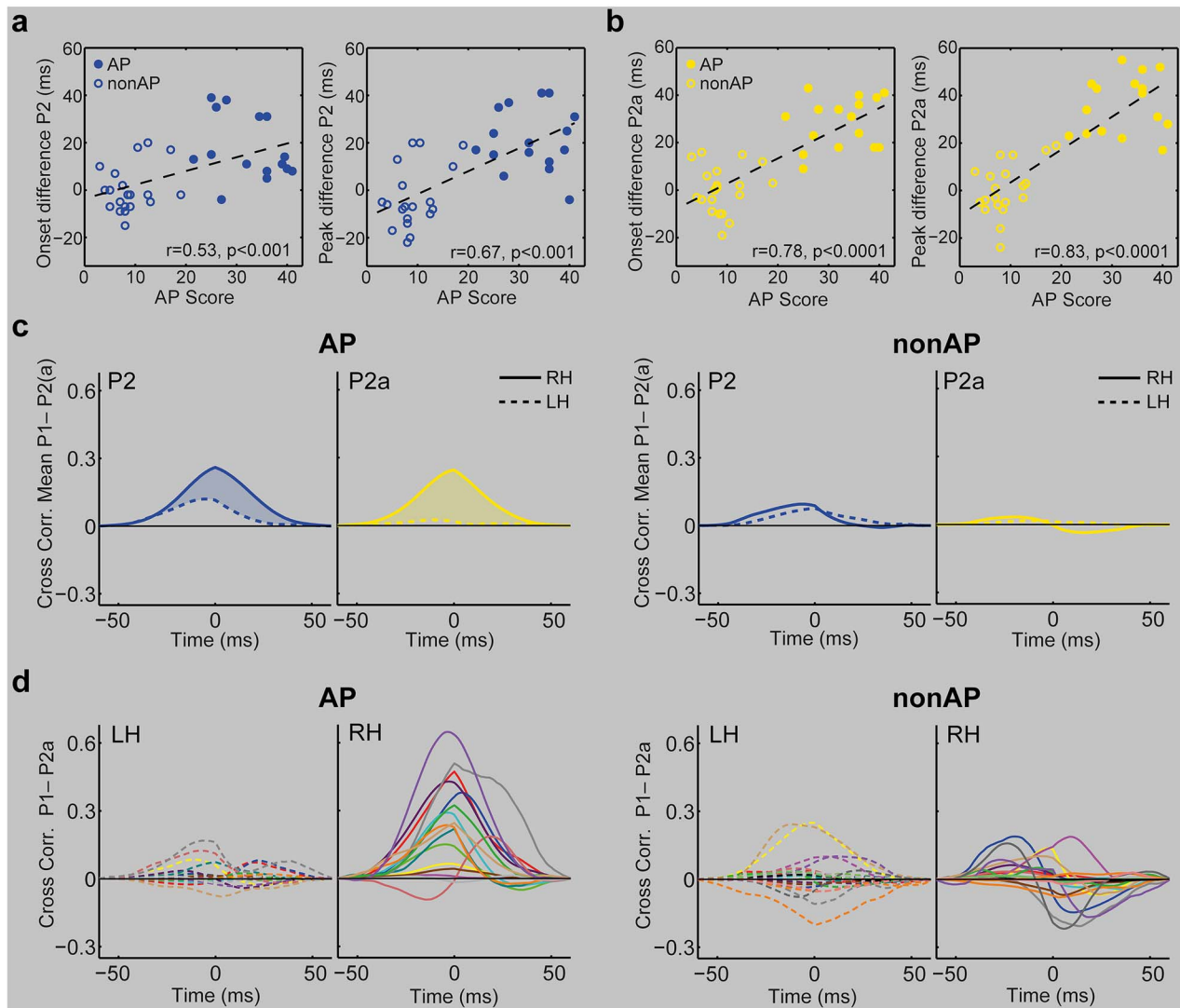
Fig. 5. The synchronization of right auditory areas correlates with AP proficiency. Left–right onset and peak differences of the a) late P2 and b) P2a responses in AC correlate significantly with the AP score and clearly differentiate both groups. c) Mean and d) individual cross-correlations of source waveforms of the early P1 with the late P2 (blue) or P2a (yellow) responses show a clear peak synchronization in the AP-group in the right hemisphere due to the preceding right P2(a) responses, in contrast to the left hemisphere and the nonAP group. AP, absolute pitch; nonAP, nonabsolute pitch; LH/RH, left/right hemisphere.

within the left and right AC, which are organized symmetrically in both hemispheres. MEG source modeling integrating the spatial information of these loci enabled the differentiation of auditory source components and the extraction of response onsets and peaks in millisecond resolution. Thus, the earliest cortical processing step occurs at around 20 ms (poststimulus onset) at the location of primary (core) AC in medial HG (Fig. 6, red region). Auditory information then extends over 5–10 ms along the medio-lateral axis toward the secondary (belt) AC in the lateral HG (green region). From here, two processing paths emerge along STG, one stream in anterior direction toward parabelt areas in anterior STG (blue region) and a second posterior processing stream toward parabelt areas in PT (yellow region). The response onsets in parabelt areas around 50–60 ms (poststimulus onset) reflect the expected latency of serial processing and the integration of cortico–cortical feedback from auditory and nonauditory areas. Accordingly, auditory responses in parabelt areas were less synchronized than those

in core and belt areas and displayed higher interindividual variability.

The results of this study were obtained in musicians, who form a special population with respect to their anatomical and functional auditory properties (Münte et al. 2002; Schneider et al. 2002; Sluming et al. 2002; Gaser and Schlaug 2003; Bangert and Schlaug 2006; Bermudez et al. 2009). The rationale behind this choice of subjects was that experienced and attentive listeners such as musicians display enhanced auditory responses in comparison to the general population. This aimed at increasing the robustness of our results. However, musical training is known to modulate neurocognitive functions in auditory and other modalities (Altenmüller and Furuya 2016). Notably, such neuroplasticity and some cognitive near and far transfer effects have been observed, be the musical training formal or informal, group-based or individual, and with early onset in childhood or later in adolescence (Habibi et al. 2018; Putkinen and Tervaniemi 2018; Criscuolo et al. 2022). Therefore,
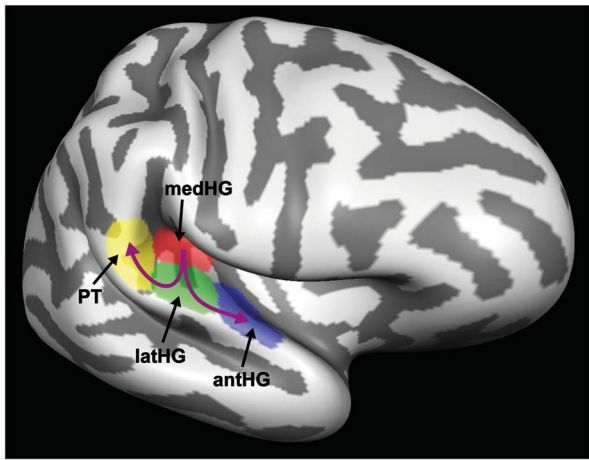
Fig. 6. Chronotopic sequence of auditory processing in AC. Schematic illustration of the core-to-belt-to-parabelt auditory processing sequence within AC, proceeding from medial HG (ROI 1, red) to lateral HG (ROI 2, green) and further splitting parallely to anterior STG (ROI 3, blue) and PT (ROI 4, yellow). medHG, medial Heschl's gyrus; latHG, lateral Heschl's gyrus; antSTG, anterior superior temporal gyrus; PT, planum temporale.

generalization of our results to the general population may be limited.

Synchronization and lateralization of auditory responses in musicians with and without AP

Hemispherical differences with respect to structure, function, and linkage of the right and left AC have extensively been discussed with respect to spatial and/or temporal aspects (Schlaug et al. 1995; Schneider et al. 2002; Boemio et al. 2005; Serrallach et al. 2016; Benner et al. 2017; Rus-Oswald et al. 2022). However, systematic co-registration of spatial and temporal information has not been undertaken, and therefore, the mechanisms of intra- and interhemispheric integration, tuning, and synchronization in human AC are not fully understood.

Our previous study combining MEG with structural as well as functional MRI revealed the correlation of AP proficiency with grey matter volume of right HG and amplitudes of AEF (Wengenroth et al. 2014). Here, we describe for the first time, characteristic variations in the temporal hierarchical order of right- and left-hemispheric auditory responses by comparing 2 cohorts of experienced musicians with and without AP. The present analysis of chronotopy in AC offers a new neurophysiological marker for the early processing stage of AP perception: the preceding response of right vs. left auditory parabelt areas leading to a specific synchronization pattern within the right AC. These results contribute to our understanding of the neurophysiological mechanisms behind auditory perception in general and AP perception in particular. The methodological approach of systematic co-registration of fMRI and MEG data emphasizes the importance of considering spatial and temporal information concomitantly in individual subjects.

AP is a rare and specific auditory ability, presumably mostly innate, which should influence early auditory processing. Moreover, since the development of the AP ability can also be considered dynamic, including contributions from individual and cultural contextual factors, AP can be seen as a model to investigate neuroplasticity of the human auditory brain (Miyazaki 1988; Miyazaki et al. 2018). In marked contrast to the nonAP group

(presumably representing the general population), musicians with AP consistently demonstrated stronger synchronization of right-hemispheric auditory responses as compared with the left hemisphere. Furthermore, auditory responses occurred more rapidly in AP musicians, e.g. ~25 ms earlier in the right as compared with the left PT and ~15 ms earlier in the right as compared with the left anterior STG. This right-hemispheric synchronization and lateralization effect was evident at the individual level and correlated strongly with AP proficiency, corroborating earlier evidence for the specific role of the right hemisphere in AP processing (Wengenroth et al. 2014; Kim and Knösche 2016, 2017; Burkhard et al. 2019; Leipold et al. 2019; Burkhard et al. 2020). In addition, auditory synchronization and response patterns showed important interindividual variations, pointing to possible neuroplastic effects at the functional level, particularly in parabelt areas. Arguably, the observed right-hemispheric synchronization of belt and parabelt areas could reflect altered neuronal connectivity in AP musicians, as suggested by previous reports (Loui et al. 2011; Jäncke et al. 2012). Developmental studies in early childhood demonstrated faster maturation of the right hemisphere as compared with the left, suggesting increased myelination of the right side at a particular age (Chi et al. 1977; Chiron et al. 1997). A right-hemispheric advantage in maturation—inherited or acquired— may have also an influence on the specific network properties in AP possessors. Or one might even envisage that altered connectivity in AP might be part of a broader developmental spectrum. For instance, it was suggested that AP individuals may also have autistic traits, i.e. AP and autism may share some neural features or connectivity patterns (Wenhart et al. 2019). However, AP ability seems to be not associated with deficits in social and communication domains that are characteristic for autism (Dohn et al. 2012).

Finally, the presented results are at the basis of the early perceptual processing stage of AP, e.g. pitch recognition. The subsequent processing stages of pitch labeling and memory require further interhemispheric interaction of parabelt areas as well as the involvement of more distant nonauditory regions such as the left prefrontal (Levitin and Rogers 2005; Elmer et al. 2015; Rogenmoser et al. 2021) and visual cortex (Greber et al. 2020). Recent studies indicate moreover the influence of large-scale brain networks (Leipold et al. 2021).

Conclusion

We employed co-registration of fMRI and MEG to achieve spatial and temporal segregation of auditory responses in musicians. For the first time, we introduce a noninvasive method which provides information about individual chronotopic response patterns. These patterns reflect the spatio–temporal hierarchical organization of distinct auditory subareas and furthermore mirror individual differences in auditory perceptual abilities. We were able to derive on the one hand a model for the general population (based on the results from nonAP musicians) and, on the other hand, use the model to investigate the specific temporal mechanism of an exceptional auditory skill (based on the results from AP musicians). Our finding of preceding responses of the right vs. left auditory parabelt areas leading to a characteristic right-hemispheric synchronization pattern in AP musicians provide the so far most comprehensive depiction of early perceptional aspects of AP processing. Taken together, auditory information processing was found to be chronotopically organized, exhibiting distinctive temporal dynamics in the presence of specific human auditory skills.

Data availability

Raw data is available from the corresponding author on reasonable request.

Conflict of interest statement: None declared.

CRediT for author contributions

Jan Benner (Data curation, Formal analysis, Investigation, Software, Validation, Visualization, Writing—original draft, Writing—review & editing), Julia Reinhardt (Data curation, Formal analysis, Investigation, Software, Visualization, Writing—review & editing), Markus Christiner (Formal analysis, Software, Validation, Writing—review & editing), Martina Wengenroth (Investigation, Visualization, Writing—original draft), Christoph Stippich (Methodology, Resources), Peter Schneider (Conceptualization, Formal analysis, Funding acquisition, Investigation, Methodology, Supervision, Validation, Writing—original draft, Writing—review & editing), and Maria Blatow (Conceptualization, Funding acquisition, Project administration, Supervision, Validation, Writing—original draft, Writing—review & editing)

References

Abdul-Kareem IA, Sluming V. Heschl gyrus and its included primary auditory cortex: Structural MRI studies in healthy and diseased subjects. *J Magn Reson Imaging*. 2008:28(2):287–299.

Allen EJ, Mesik J, Kay KN, Oxenham AJ. Distinct representations of tonotopy and pitch in human auditory cortex. *J Neurosci*. 2022:42(3):416–434.

Altenmüller E, Furuya S. Brain plasticity and the concept of metaplasticity in skilled musicians. In: Laczko J, Latash ML, editors. *Progress in Motor Control* Cham: Springer; 2016, p. 197–208.

Baharloo S, Johnston PA, Service SK, Gitschier J, Freimer NB. Absolute pitch: an approach for identification of genetic and nongenetic components. *Am J Hum Genet*. 1998:62(2):224–231.

Bangert M, Schlaug G. Specialization of the specialized in features of external human brain morphology. *Eur J Neurosci*. 2006:24(6): 1832–1834.

Barton B, Venezia JH, Saberi K, Hickok G, Brewer AA. Orthogonal acoustic dimensions define auditory field maps in human cortex. *Proc Natl Acad Sci U S A*. 2012:109(50):20738–20743.

Behne N, Scheich H, Brechmann A. Contralateral white noise selectively changes right human auditory cortex activity caused by a FM-direction task. *J Neurophysiol*. 2005:93(1):414–423.

Benner J, Wengenroth M, Reinhardt J, Stippich C, Schneider P, Blatow M. Prevalence and function of Heschl's gyrus morphotypes in musicians. *Brain Struct Funct*. 2017:222(8):3587–3603.

Bermudez P, Lerch JP, Evans AC, Zatorre RJ. Neuroanatomical correlates of musicianship as revealed by cortical thickness and voxel-based morphometry. *Cereb Cortex*. 2009:19(7):1583–1596.

Bermudez P, Zatorre RJ. Conditional associative memory for musical stimuli in nonmusicians: Implications for absolute pitch. *J Neurosci*. 2005:25(34):7718–7723.

Besle J, Mougin O, Sanchez-Panchuelo RM, Lanting C, Gowland P, Bowtell R, Francis S, Krumbholz K. Is human auditory cortex organization compatible with the monkey model? Contrary evidence from ultra-high-field functional and structural MRI. *Cereb Cortex*. 2019:29(1):410–428.

Bilecen D, Scheffler K, Schmid N, Tschopp K, Seelig J. Tonotopic organization of the human auditory cortex as detected by BOLD-FMRI. *Hear Res*. 1998:126(1–2):19–27.

Bilecen D, Seifritz E, Scheffler K, Henning J, Schulte AC. Amplitopicity of the human auditory cortex: An fMRI study. *NeuroImage*. 2002:17(2):710–718.

Binder JR, Frost JA, Hammeke TA, Bellgowan PS, Springer JA, Kaufman JN, Possing ET. Human temporal lobe activation by speech and nonspeech sounds. *Cereb Cortex*. 2000:10(5):512–528.

Blatow M, Nennig E, Durst A, Sartor K, Stippich C. fMRI reflects functional connectivity of human somatosensory cortex. *NeuroImage*. 2007:37(3):927–936.

Blatow M, Nennig E, Sarpaczki E, Reinhardt J, Schlieter M, Herweh C, Rasche D, Tronnier VM, Sartor K, Stippich C. Altered somatosensory processing in trigeminal neuralgia. *Hum Brain Mapp*. 2009:30(11):3495–3508.

Blatow M, Reinhardt J, Riffel K, Nennig E, Wengenroth M, Stippich C. Clinical functional MRI of sensorimotor cortex using passive motor and sensory stimulation at 3 Tesla. *J Magn Reson Imaging*. 2011:34(2):429–437.

Boemio A, Fromm S, Braun A, Poeppel D. Hierarchical and asymmetric temporal sensitivity in human auditory cortices. *Nat Neurosci*. 2005:8(3):389–395.

Brugge JF, Volkov IO, Oya H, Kawasaki H, Reale RA, Fenoy A, Steinschneider M, Howard MA 3rd. Functional localization of auditory cortical fields of human: click-train stimulation. *Hear Res*. 2008:238(1–2):12–24.

Burkhard A, Elmer S, Jäncke L. Early tone categorization in absolute pitch musicians is subserved by the right-sided perisylvian brain. *Sci Rep*. 2019:9(1):1419.

Burkhard A, Hänggi J, Elmer S, Jäncke L. The importance of the fibre tracts connecting the planum temporale in absolute pitch possessors. *NeuroImage*. 2020:211:116590.

Camalier CR, D'Angelo WR, Sterbing-D'Angelo SJ, de la Mothe LA, Hackett TA. Neural latencies across auditory cortex of macaque support a dorsal stream supramodal timing advantage in primates. *Proc Natl Acad Sci U S A*. 2012:109(44): 18168–18173.

Chevillet M, Riesenhuber M, Rauschecker JP. Functional correlates of the anterolateral processing hierarchy in human auditory cortex. *J Neurosci*. 2011:31(25):9345–9352.

Chi JG, Dooling EC, Gilles FH. Gyral development of the human brain. *Ann Neurol*. 1977:1(1):86–93.

Chiron C, Jambaque I, Nabbout R, Lounes R, Syrota A, Dulac O. The right brain hemisphere is dominant in human infants. *Brain*. 1997:120(6):1057–1065.

Coffey EBJ, Musacchia G, Zatorre RJ. Cortical correlates of the auditory frequency-following and onset responses: EEG and fMRI evidence. *J Neurosci*. 2017:37(4):830–838.

Coll SY, Vuichoud N, Grandjean D, James CE. Electrical neuroimaging of music processing in pianists with and without true absolute pitch. *Front Neurosci.* 2019:13:142.

Criscuolo A, Pando-Naude V, Bonetti L, Vuust P, Brattico E. An ALE meta-analytic review of musical expertise. *Sci Rep.* 2022:12(1):11726.

Da Costa S, van der Zwaag W, Marques JP, Frackowiak RS, Clarke S, Saenz M. Human primary auditory cortex follows the shape of Heschl's gyrus. *J Neurosci.* 2011:31(40):14067–14075.

De Martino F, Moerel M, Xu J, van de Moortele PF, Ugurbil K, Goebel R, Yacoub E, Formisano E. High-resolution mapping of myeloarchitecture in vivo: localization of auditory areas in the human brain. *Cereb Cortex.* 2015:25(10):3394–3405.

Dohn A, Garza-Villarreal EA, Chakravarty MM, Hansen M, Lerch JP, Vuust P. Gray- and white-matter anatomy of absolute pitch possessors. *Cereb Cortex.* 2015:25(5):1379–1388.

Dohn A, Garza-Villarreal EA, Heaton P, Vuust P. Do musicians with perfect pitch have more autism traits than musicians without perfect pitch? An empirical study. *PLoS One.* 2012:7(5):e37961.

Elmer S, Rogenmoser L, Kuhnis J, Jäncke L. Bridging the gap between perceptual and cognitive perspectives on absolute pitch. *J Neurosci.* 2015:35(1):366–371.

Farbood MM, Heeger DJ, Marcus G, Hasson U, Lerner Y. The neural processing of hierarchical structure in music and speech at different timescales. *Front Neurosci.* 2015:9:157.

Formisano E, Kim DS, Di Salle F, van de Moortele PF, Ugurbil K, Goebel R. Mirror-symmetric tonotopic maps in human primary auditory cortex. *Neuron.* 2003:40(4):859–869.

Fullerton BC, Pandya DN. Architectonic analysis of the auditory-related areas of the superior temporal region in human brain. *J Comp Neurol.* 2007:504(5):470–498.

Galaburda A, Sanides F. Cytoarchitectonic organization of the human auditory cortex. *J Comp Neurol.* 1980:190(3):597–610.

Gaser C, Schlaug G. Brain structures differ between musicians and non-musicians. *J Neurosci.* 2003:23(27):9240–9245.

Glasser MF, Coalson TS, Robinson EC, Hacker CD, Harwell J, Yacoub E, Ugurbil K, Andersson J, Beckmann CF, Jenkinson M, et al. A multi-modal parcellation of human cerebral cortex. *Nature.* 2016:536(7615):171–178.

Godey B, Schwartz D, de Graaf JB, Chauvel P, Liegeois-Chauvel C. Neuromagnetic source localization of auditory evoked fields and intracerebral evoked potentials: a comparison of data in the same patients. *Clin Neurophysiol.* 2001:112(10):1850–1859.

Golestani N, Price CJ, Scott SK. Born with an ear for dialects? Structural plasticity in the expert phonetician brain. *J Neurosci.* 2011:31(11):4213–4220.

Gordon EE. *Introduction to research and the psychology of music.* Chicago: GIA, 1998.

Greber M, Klein C, Leipold S, Sele S, Jäncke L. Heterogeneity of EEG resting-state brain networks in absolute pitch. *Int J Psychophysiol.* 2020:157:11–22.

Greber M, Rogenmoser L, Elmer S, Jäncke L. Electrophysiological correlates of absolute pitch in a passive auditory oddball paradigm: a direct replication attempt. *eNeuro.* 2018:5(6):ENEURO.0333–ENEU18.2018.

Gregersen PK, Kowalsky E, Kohn N, Marvin EW. Absolute pitch: prevalence, ethnic variation, and estimation of the genetic component. *Am J Hum Genet.* 1999:65(3):911–913.

Griffiths TD. Functional imaging of pitch analysis. *Ann N Y Acad Sci.* 2003:999(1):40–49.

Gruhn W. How stable is pitch labeling accuracy in absolute pitch possessors? *Empir Musicol Rev.* 2018:13:110–123.

Gulban OF, Goebel R, Moerel M, Zachlod D, Mohlberg H, Amunts K, de Martino F. Improving a probabilistic cytoarchitectonic atlas of auditory cortex using a novel method for inter-individual alignment. *elife.* 2020:9:e56963.

Habibi A, Damasio A, Ilari B, Elliott Sachs M, Damasio H. Music training and child development: a review of recent findings from a longitudinal study. *Ann N Y Acad Sci.* 2018:1423(1):73–81.

Hackett TA. Anatomical organization of the auditory cortex. *J Am Acad Audiol.* 2008:19(10):774–779.

Hackett TA. Information flow in the auditory cortical network. *Hear Res.* 2011:271(1–2):133–146.

Hackett TA, de la Mothe LA, Camalier CR, Falchier A, Lakatos P, Kajikawa Y, Schroeder CE. Feedforward and feedback projections of caudal belt and parabelt areas of auditory cortex: refining the hierarchical model. *Front Neurosci.* 2014:8:72.

Hackett TA, Preuss TM, Kaas JH. Architectonic identification of the core region in auditory cortex of macaques, chimpanzees, and humans. *J Comp Neurol.* 2001:441(3):197–222.

Hall DA, Johnsrude IS, Haggard MP, Palmer AR, Akeroyd MA, Summerfield AQ. Spectral and temporal processing in human auditory cortex. *Cereb Cortex.* 2002:12(2):140–149.

Hall EL, Robson SE, Morris PG, Brookes MJ. The relationship between MEG and fMRI. *NeuroImage.* 2014:102:80–91.

Hamilton LS, Oganian Y, Hall J, Chang EF. Parallel and distributed encoding of speech across human auditory cortex. *Cell.* 2021:184(18):4626, e4613–4626, e4639.

Herdener M, Esposito F, Scheffler K, Schneider P, Logothetis NK, Uludag K, Kayser C. Spatial representations of temporal and spectral sound cues in human auditory cortex. *Cortex.* 2013:49:2822–2833.

Hickok G, Poeppel D. The cortical organization of speech processing. *Nat Rev Neurosci.* 2007:8(5):393–402.

Howard MA, Volkov IO, Abbas PJ, Damasio H, Ollendieck MC, Granner MA. A chronic microelectrode investigation of the tonotopic organization of human auditory cortex. *Brain Res.* 1996:724(2):260–264.

Jäncke L, Langer N, Hänggi J. Diminished whole-brain but enhanced peri-sylvian connectivity in absolute pitch musicians. *J Cogn Neurosci.* 2012:24(6):1447–1461.

Jäncke L, Wustenberg T, Schulze K, Heinze HJ. Asymmetric hemodynamic responses of the human auditory cortex to monaural and binaural stimulation. *Hear Res.* 2002:170(1–2):166–178.

Joly O, Baumann S, Balezeau F, Thiele A, Griffiths TD. Merging functional and structural properties of the monkey auditory cortex. *Front Neurosci.* 2014:8:198.

Kaas JH, Hackett TA. Subdivisions of auditory cortex and processing streams in primates. *Proc Natl Acad Sci U S A.* 2000:97(22):11793–11799.

Kaas JH, Hackett TA, Tramo MJ. Auditory processing in primate cerebral cortex. *Curr Opin Neurobiol.* 1999:9(2):164–170.

Kanno A, Nakasato N, Fujita S, Seki K, Kawamura T, Ohtomo S, Fujiwara S, Yoshimoto T. Right hemispheric dominance in the auditory evoked magnetic fields for pure-tone stimuli. *Electroencephalogr Clin Neurophysiol Suppl.* 1996:47:129–132.

Keenan JP, Thangaraj V, Halpern AR, Schlaug G. Absolute pitch and planum temporale. *NeuroImage.* 2001:14(6):1402–1408.

Kim JJ, Crespo-Facorro B, Andreasen NC, O'Leary DS, Zhang B, Harris G, Magnotta VA. An MRI-based parcellation method for the temporal lobe. *NeuroImage.* 2000:11(4):271–288.

Kim SG, Knösche TR. Intracortical myelination in musicians with absolute pitch: Quantitative morphometry using 7-T MRI. *Hum Brain Mapp.* 2016:37(10):3486–3501.

Kim SG, Knösche TR. Resting state functional connectivity of the ventral auditory pathway in musicians with absolute pitch. *Hum Brain Mapp*. 2017:38(8):3899–3916.

Kwon H, Lee YH, Kim JM, Park YK, Kuriki S. Localization accuracy of single current dipoles from tangential components of auditory evoked fields. *Phys Med Biol*. 2002:47(23):4145–4154.

Lakatos P, Pincze Z, Fu KM, Javitt DC, Karmos G, Schroeder CE. Timing of pure tone and noise-evoked responses in macaque auditory cortex. *Neuroreport*. 2005:16(9):933–937.

Leaver AM, Rauschecker JP. Functional topography of human auditory cortex. *J Neurosci*. 2016:36(4):1416–1428.

Lehongre K, Morillon B, Giraud AL, Ramus F. Impaired auditory sampling in dyslexia: Further evidence from combined fMRI and EEG. *Front Hum Neurosci*. 2013:7:454.

Leipold S, Klein C, Jäncke L. Musical expertise shapes functional and structural brain networks independent of absolute pitch ability. *J Neurosci*. 2021:41(11):2496–2511.

Leipold S, Oderbolz C, Greber M, Jäncke L. A reevaluation of the electrophysiological correlates of absolute pitch and relative pitch: no evidence for an absolute pitch-specific negativity. *Int J Psychophysiol*. 2019:137:21–31.

Leonard CM, Puranik C, Kuldau JM, Lombardino LJ. Normal variation in the frequency and location of human auditory cortex landmarks. Heschl's gyrus: where is it? *Cereb Cortex*. 1998:8(5):397–406.

Levitin DJ, Rogers SE. Absolute pitch: perception, coding, and controversies. *Trends Cogn Sci*. 2005:9(1):26–33.

Liegeois-Chauvel C, Musolino A, Badier JM, Marquis P, Chauvel P. Evoked potentials recorded from the auditory cortex in man: evaluation and topography of the middle latency components. *Electroencephalogr Clin Neurophysiol*. 1994:92(3):204–214.

Loui P, Li HC, Hohmann A, Schlaug G. Enhanced cortical connectivity in absolute pitch musicians: a model for local hyperconnectivity. *J Cogn Neurosci*. 2011:23(4):1015–1026.

Luders E, Gaser C, Jäncke L, Schlaug G. A voxel-based approach to gray matter asymmetries. *NeuroImage*. 2004:22(2):656–664.

Lütkenhöner B, Krumbholz K, Seither-Preisler A. Studies of tonotopy based on wave N100 of the auditory evoked field are problematic. *NeuroImage*. 2003:19(3):935–949.

Marie D, Jobard G, Crivello F, Perchey G, Petit L, Mellet E, Joliot M, Zago L, Mazoyer B, Tzourio-Mazoyer N. Descriptive anatomy of Heschl's gyri in 430 healthy volunteers, including 198 left-handers. *Brain Struct Funct*. 2015:220(2):729–743.

Melcher JR, Talavage TM, Harms MP. Functional MRI of the auditory system. In: Mct, W. BP, A. editors. *Functional MRI*. Mauer: Springer; 1999, p. 393–406

Miyazaki K. Musical pitch identification by absolute pitch possessors. *Percept Psychophys*. 1988:44(6):501–512.

Miyazaki K, Rakowski A, Makomaska S, Jiang C, Tsuzaki M, Oxenham AJ, Ellis G, Lipscomb SD. Absolute pitch and relative pitch in music students in the east and the west. *Music Percept*. 2018:36(2):135–155.

Moerel M, De Martino F, Formisano E. Processing of natural sounds in human auditory cortex: tonotopy, spectral tuning, and relation to voice sensitivity. *J Neurosci*. 2012:32(41):14205–14216.

Moerel M, De Martino F, Formisano E. An anatomical and functional topography of human auditory cortical areas. *Front Neurosci*. 2014:8:225.

Moerel M, Yacoub E, Gulban OF, Lage-Castellanos A, De Martino F. Using high spatial resolution fMRI to understand representation in the auditory network. *Prog Neurobiol*. 2021:207:101887.

Morel A, Garraghty PE, Kaas JH. Tonotopic organization, architectonic fields, and connections of auditory cortex in macaque monkeys. *J Comp Neurol*. 1993:335(3):437–459.

Morosan P, Rademacher J, Schleicher A, Amunts K, Schormann T, Zilles K. Human primary auditory cortex: cytoarchitectonic subdivisions and mapping into a spatial reference system. *NeuroImage*. 2001:13(4):684–701.

Münte TF, Altenmüller E, Jäncke L. The musician's brain as a model of neuroplasticity. *Nat Rev Neurosci*. 2002:3(6):473–478.

Nourski KV. Auditory processing in the human cortex: an intracranial electrophysiology perspective. *Laryngoscope Investig Otolaryngol*. 2017:2(4):147–156.

Nourski KV, Steinschneider M, McMurray B, Kovach CK, Oya H, Kawasaki H, Howard MA 3rd. Functional organization of human auditory cortex: investigation of response latencies through direct recordings. *NeuroImage*. 2014:101:598–609.

Oechslin MS, Meyer M, Jäncke L. Absolute pitch–functional evidence of speech-relevant auditory acuity. *Cereb Cortex*. 2010:20(2):447–455.

Ohnishi T, Matsuda H, Asada T, Aruga M, Hirakata M, Nishikawa M, Katoh A, Imabayashi E. Functional anatomy of musical perception in musicians. *Cereb Cortex*. 2001:11(8):754–760.

Okada K, Rong F, Venezia J, Matchin W, Hsieh IH, Saberi K, Serences JT, Hickok G. Hierarchical organization of human auditory cortex: evidence from acoustic invariance in the response to intelligible speech. *Cereb Cortex*. 2010:20(10):2486–2495.

Okamoto H, Stracke H, Draganova R, Pantev C. Hemispheric asymmetry of auditory evoked fields elicited by spectral versus temporal stimulus change. *Cereb Cortex*. 2009:19(10):2290–2297.

Okamoto H, Teismann H, Kakigi R, Pantev C. Auditory evoked fields elicited by spectral, temporal, and spectral-temporal changes in human cerebral cortex. *Front Psychol*. 2012:3:149.

Pantev C, Bertrand O, Eulitz C, Verkindt C, Hampson S, Schuierer G, Elbert T. Specific tonotopic organizations of different areas of the human auditory cortex revealed by simultaneous magnetic and electric recordings. *Electroencephalogr Clin Neurophysiol*. 1995:94(1):26–40.

Pantev C, Hoke M, Lehnertz K, Lutkenhoner B, Anogianakis G, Wittkowski W. Tonotopic organization of the human auditory cortex revealed by transient auditory evoked magnetic fields. *Electroencephalogr Clin Neurophysiol*. 1988:69(2):160–170.

Pantev C, Hoke M, Lutkenhoner B, Lehnertz K. Tonotopic organization of the auditory cortex: pitch versus frequency representation. *Science*. 1989:246(4929):486–488.

Patterson RD, Uppenkamp S, Johnsrude IS, Griffiths TD. The processing of temporal pitch and melody information in auditory cortex. *Neuron*. 2002:36(4):767–776.

Peeters R, Sunaert S. Clinical bold fMRI: artifacts, tips and tricks. In: Stippich C, editor. *Clinical Functional MRI*. Berlin, Heidelberg: Springer; 2007, p. 227–249.

Penhune VB, Cismaru R, Dorsaint-Pierre R, Petitto LA, Zatorre RJ. The morphometry of auditory cortex in the congenitally deaf measured using MRI. *NeuroImage*. 2003:20(2):1215–1225.

Penhune VB, Zatorre RJ, MacDonald JD, Evans AC. Interhemispheric anatomical differences in human primary auditory cortex: probabilistic mapping and volume measurement from magnetic resonance scans. *Cereb Cortex*. 1996:6(5):661–672.

Petkov CI, Kang X, Alho K, Bertrand O, Yund EW, Woods DL. Attentional modulation of human auditory cortex. *Nat Neurosci*. 2004:7(6):658–663.

Pfeifer RA. Pathologie der Hörstrahlung und der corticalen Hörsphäre. In: Bumke O, Foerster O, editors. Handbuch der Neurologie. Berlin: Springer; 1936, p. 533–626.

Putkinen V, Tervaniemi M. Neuroplasticity in music learning. In: Thaut MH, Hodges DA, editors. *The Oxford Handbook of Music and the Brain*. Oxford University Press; 2019, p. 545–563.

Rademacher J, Caviness VS Jr, Steinmetz H, Galaburda AM. Topographical variation of the human primary cortices: Implications for neuroimaging, brain mapping, and neurobiology. *Cereb Cortex*. 1993:3(4):313–329.

Rademacher J, Morosan P, Schormann T, Schleicher A, Werner C, Freund HJ, Zilles K. Probabilistic mapping and volume measurement of human primary auditory cortex. *NeuroImage*. 2001:13(4):669–683.

Rauschecker JP. Cortical processing of complex sounds. *Curr Opin Neurobiol*. 1998:8(4):516–521.

Rauschecker JP, Tian B, Hauser M. Processing of complex sounds in the macaque nonprimary auditory cortex. *Science*. 1995:268(5207):111–114.

Recanzone GH, Guard DC, Phan ML. Frequency and intensity response properties of single neurons in the auditory cortex of the behaving macaque monkey. *J Neurophysiol*. 2000:83(4):2315–2331.

Reite M, Teale P, Rojas DC, Reite E, Asherin R, Hernandez O. MEG auditory evoked fields suggest altered structural/functional asymmetry in primary but not secondary auditory cortex in bipolar disorder. *Bipolar Disord*. 2009:11(4):371–381.

Reymore L, Hansen NC. A theory of instrument-specific absolute pitch. *Front Psychol*. 2020:11:560877.

Rogenmoser L, Arnicane A, Jäncke L, Elmer S. The left dorsal stream causally mediates the tone labeling in absolute pitch. *Ann N Y Acad Sci*. 2021:1500(1):122–133.

Rogenmoser L, Elmer S, Jäncke L. Absolute pitch: evidence for early cognitive facilitation during passive listening as revealed by reduced P3a amplitudes. *J Cogn Neurosci*. 2015:27(3):623–637.

Romani GL, Williamson SJ, Kaufman L. Tonotopic organization of the human auditory cortex. *Science*. 1982:216(4552):1339–1340.

Romanski LM, Tian B, Fritz J, Mishkin M, Goldman-Rakic PS, Rauschecker JP. Dual streams of auditory afferents target multiple domains in the primate prefrontal cortex. *Nat Neurosci*. 1999:2(12):1131–1136.

Ruggles DR, Tausend AN, Shamma SA, Oxenham AJ. Cortical markers of auditory stream segregation revealed for streaming based on tonotopy but not pitch. *J Acoust Soc Am*. 2018:144(4):2424–2433.

Rus-Oswald OG, Benner J, Reinhardt J, Burki C, Christiner M, Hofmann E, Schneider P, Stippich C, Kressig RW, Blatow M. Musicianship-related structural and functional cortical features are preserved in elderly musicians. *Front Aging Neurosci*. 2022:14:807971.

Saenz M, Langers DR. Tonotopic mapping of human auditory cortex. *Hear Res*. 2014:307:42–52.

Scheich H, Baumgart F, Gaschler-Markefski B, Tegeler C, Tempelmann C, Heinze HJ, Schindler F, Stiller D. Functional magnetic resonance imaging of a human auditory cortex area involved in foreground-background decomposition. *Eur J Neurosci*. 1998:10(2):803–809.

Scherg M. Spatio-temporal modelling of early auditory evoked potentials. *Rev Laryngol Otol Rhinol (Bord)*. 1984:105(2 Suppl):163–170.

Scherg M. *Fundamentals of dipole source potential analysis*. In: Grandori F, Hoke M, Romani GI, editors. Auditory evoked magnetic fields and electric potentials. Basel: Karger; 1990, p. 40–69.

Scherg M, Berg P. Use of prior knowledge in brain electromagnetic source analysis. *Brain Topogr*. 1991:4(2):143–150.

Scherg M, Berg P. New concepts of brain source imaging and localization. *Electroencephalogr Clin Neurophysiol Suppl*. 1996:46:127–137.

Scherg M, Hari R, Hämäläinen M. Frequency-specific sources of the Auditory N19-P30-P50 response detected by a multiple source analysis of evoked magnetic fields and potentials. In: Williamson SJ, Hoke M, Stroink G, Kotani M, editors. *Advances in Biomagnetism*. Boston, MA: Springer US; 1989, p. 97–100.

Schlaug G, Jäncke L, Huang Y, Steinmetz H. In vivo evidence of structural brain asymmetry in musicians. *Science*. 1995:267(5198):699–701.

Schneider P, Andermann M, Wengenroth M, Goebel R, Flor H, Rupp A, Diesch E. Reduced volume of Heschl's gyrus in tinnitus. *NeuroImage*. 2009:45(3):927–939.

Schneider P, Scherg M, Dosch HG, Specht HJ, Gutschalk A, Rupp A. Morphology of Heschl's gyrus reflects enhanced activation in the auditory cortex of musicians. *Nat Neurosci*. 2002:5(7):688–694.

Schneider P, Sluming V, Roberts N, Scherg M, Goebel R, Specht HJ, Dosch HG, Bleeck S, Stippich C, Rupp A. Structural and functional asymmetry of lateral Heschl's gyrus reflects pitch perception preference. *Nat Neurosci*. 2005:8(9):1241–1247.

Schreiner CE, Winer JA. Auditory cortex mapmaking: principles, projections, and plasticity. *Neuron*. 2007:56(2):356–365.

Schulze K, Gaab N, Schlaug G. Perceiving pitch absolutely: comparing absolute and relative pitch possessors in a pitch memory task. *BMC Neurosci*. 2009:10(1):106.

Seifritz E, Esposito F, Hennel F, Mustovic H, Neuhoff JG, Bilecen D, Tedeschi G, Scheffler K, Di Salle F. Spatiotemporal pattern of neural processing in the human auditory cortex. *Science*. 2002:297(5587):1706–1708.

Seither-Preisler A, Parncutt R, Schneider P. Size and synchronization of auditory cortex promotes musical, literacy, and attentional skills in children. *J Neurosci*. 2014:34(33):10937–10949.

Serrallach B, Gross C, Bernhofs V, Engelmann D, Benner J, Gundert N, Blatow M, Wengenroth M, Seitz A, Brunner M, et al. Neural biomarkers for dyslexia, ADHD, and ADD in the auditory cortex of children. *Front Neurosci*. 2016:10:324.

Shaw ME, Hamalainen MS, Gutschalk A. How anatomical asymmetry of human auditory cortex can lead to a rightward bias in auditory evoked fields. *NeuroImage*. 2013:74:22–29.

Sluming V, Barrick T, Howard M, Cezayirli E, Mayes A, Roberts N. Voxel-based morphometry reveals increased gray matter density in Broca's area in male symphony orchestra musicians. *NeuroImage*. 2002:17(3):1613–1622.

Steinmetz H, Rademacher J, Huang YX, Hefter H, Zilles K, Thron A, Freund HJ. Cerebral asymmetry: MR planimetry of the human planum temporale. *J Comput Assist Tomogr*. 1989:13(6):996–1005.

Stippich C, Blatow M, Durst A, Dreyhaupt J, Sartor K. Global activation of primary motor cortex during voluntary movements in man. *NeuroImage*. 2007:34(3):1227–1237.

Sweet RA, Dorph-Petersen KA, Lewis DA. Mapping auditory core, lateral belt, and parabelt cortices in the human superior temporal gyrus. *J Comp Neurol*. 2005:491(3):270–289.

Talairach J, Tournoux P. *Co-planar stereotaxic atlas of the human brain: 3-dimensional proportional system : an approach to cerebral imaging*. Stuttgart; New York: Georg Thieme; 1988.

Talavage TM, Sereno MI, Melcher JR, Ledden PJ, Rosen BR, Dale AM. Tonotopic organization in human auditory cortex revealed by progressions of frequency sensitivity. *J Neurophysiol*. 2004:91(3):1282–1296.

Tang H, Crain S, Johnson BW. Dual temporal encoding mechanisms in human auditory cortex: Evidence from MEG and EEG. *NeuroImage*. 2016:128:32–43.

Wengenroth M, Blatow M, Bendszus M, Schneider P. Leftward lateralization of auditory cortex underlies holistic sound perception in Williams syndrome. *PLoS One*. 2010:5(8):e12326.

Wengenroth M, Blatow M, Heinecke A, Reinhardt J, Stippich C, Hofmann E, Schneider P. Increased volume and function of right

auditory cortex as a marker for absolute pitch. *Cereb Cortex.* 2014:24(5):1127–1137.

Wenhart T, Bethlehem RAI, Baron-Cohen S, Altenmüller E. Autistic traits, resting-state connectivity, and absolute pitch in professional musicians: shared and distinct neural features. *Mol Autism.* 2019:10(1):20.

Wessinger CM, VanMeter J, Tian B, Van Lare J, Pekar J, Rauschecker JP. Hierarchical organization of the human auditory cortex revealed by functional magnetic resonance imaging. *J Cogn Neurosci.* 2001:13(1):1–7.

Wienbruch C, Paul I, Weisz N, Elbert T, Roberts LE. Frequency organization of the 40-Hz auditory steady-state response in normal hearing and in tinnitus. *NeuroImage.* 2006:33(1):180–194.

Wilson SJ, Lusher D, Wan CY, Dudgeon P, Reutens DC. The neurocognitive components of pitch processing: Insights from absolute pitch. *Cereb Cortex.* 2009:19(3):724–732.

Wong PC, Warrier CM, Penhune VB, Roy AK, Sadehh A, Parrish TB, Zatorre RJ. Volume of left Heschl's gyrus and linguistic pitch learning. *Cereb Cortex.* 2008:18(4):828–836.

Woods DL, Alain C. Functional imaging of human auditory cortex. *Curr Opin Otolaryngol Head Neck Surg.* 2009:17(5):407–411.

Woods DL, Stecker GC, Rinne T, Herron TJ, Cate AD, Yund EW, Liao I, Kang X. Functional maps of human auditory cortex: effects of acoustic features and attention. *PLoS One.* 2009:4(4):e5183.

Yoshiura T, Higano S, Rubio A, Shrier DA, Kwok WE, Iwanaga S, Numaguchi Y. Heschl and superior temporal gyri: low signal intensity of the cortex on T2-weighted MR images of the normal brain. *Radiology.* 2000:214(1):217–221.

Yoshiura T, Ueno S, Iramina K, Masuda K. Source localization of middle latency auditory evoked magnetic fields. *Brain Res.* 1995: 703(1–2):139–144.

Yoshiura T, Ueno S, Iramina K, Masuda K. Human middle latency auditory evoked magnetic fields. *Brain Topogr.* 1996:8(3): 291–296.

Yvert B, Fischer C, Bertrand O, Pernier J. Localization of human supratemporal auditory areas from intracerebral auditory evoked potentials using distributed source models. *NeuroImage.* 2005:28(1):140–153.

Zatorre RJ. Absolute pitch: a model for understanding the influence of genes and development on neural and cognitive function. *Nat Neurosci.* 2003:6(7):692–695.

Zatorre RJ, Belin P, Penhune VB. Structure and function of auditory cortex: music and speech. *Trends Cogn Sci.* 2002:6(1):37–46.

Zatorre RJ, Perry DW, Beckett CA, Westbury CF, Evans AC. Functional anatomy of musical processing in listeners with absolute pitch and relative pitch. *Proc Natl Acad Sci U S A.* 1998:95(6): 3172–3177.

Zoellner S, Benner J, Zeidler B, Seither-Preisler A, Christiner M, Seitz A, Goebel R, Heinecke A, Wengenroth M, Blatow M, et al. Reduced cortical thickness in Heschl's gyrus as an in vivo marker for human primary auditory cortex. *Hum Brain Mapp.* 2019:40(4): 1139–1154.